# EUMETSAT / ECMWF

# Fellowship Programme

Research Report No. 10

# Monitoring of METEOSAT WV Radiances and Solar Stray Light Effects

**C. Köpken**

September 2001

**Abstract**

Radiances in the WV and IR channels of the Meteosat–5 and Meteosat–7 satellites are being continuously monitored in the form of hourly clear–sky radiances using the operational ECMWF data assimilation system. Here, monitoring results of a one year period, April 2000 to Match 2001, are discussed concentrating on the stability of the calibration and anomalous effects caused by solar stray light in some images close to midnight. Results show that the introduction of the blackbody calibration for Meteosat–7 on 29 May 2000 has led to stable radiances. Before, and for Meteosat–5 until the introduction of a cross–calibration to Meteosat–7 on 31 May 2001, variations of about 2–4 K occur on short time scales, sometimes even within one day. The use of the on board blackbody results in a considerably more stable calibration, only minor variations of about 0.5 K being observed as a slow up and downwards drift. Monitoring time series at hourly resolution further show that anomalies are present in some images close to midnight, particularly strong effects being observed close to the eclipse seasons. The effects are caused by solar stray light entering the radiometer creating different anomaly patterns like warm bows, small very intense warm spots, warm and cold horizontal stripes and too cold calibration of large parts of certain images. Far from eclipse season, warm bows are present in the 01 UTC data having an amplitude of 2–4 K. But in extreme cases, close to eclipse, local anomalies may exceed 10–25 K. Data at 23 UTC, 00 UTC, 01 UTC, 02 UTC, and 03 UTC are affected to a different extent and at different times. Some of the slots are shown to be contaminated for considerable periods before and after the spring and autumn eclipses.

# 1 Introduction

Atmospheric data assimilation systems like the four–dimensional variational assimilation (4DVAR) used at ECMWF analyze operationally observations from many different sources including radiances measured by several instruments on different satellite platforms. During the analysis process, the measurements are compared to the model fields. This is not only done for the observations used actively in the analysis, but also for other available measurements that may thus be 'passively' monitored. This data monitoring serves a twofold purpose: One is to control the model's ability to reproduce the observed atmospheric state, which is important especially for assessing benefits of model changes. But reciprocally, the comparison of observations to the model analyses and short range forecasts allows a control of the measurements themselves and helps particularly in detecting gross errors or systematic problems in the data.

This second aspect is exploited here. Monitoring results for the radiances of the water vapour channel (WV) of the three channel imaging radiometer called MVIRI (Meteosat Visible and Infrared Radiation Imager) on board of the Meteosat–5 and Meteosat–7 (MET–5 and MET–7, respectively) are discussed. The monitoring time series based on hourly data allow especially to detect systematic biases, instabilities or diurnal characteristics in the radiances and even local anomalies. Results for MET–5 and MET–7 taken from the one year period April 2000 to March 2001 are presented and discussed showing a range of characteristics that may be seen in careful monitoring. A detailed study of the radiance quality is done for the more stably

calibrated MET–7. While the question of the observed bias was addressed in more detail in Köpken (2001), the current study concentrates on anomalous effects in the radiances caused by solar stray light and the stability of the blackbody calibration. The occurrence and location of anomalies caused by solar stray light is described in detail giving examples of effects occurring at different times throughout the year and also using time series. The purpose of this work is to give some detailed monitoring feedback to EUMETSAT which may help in further improving the WV data quality and especially for introducing a flagging mechanism to mark the areas or slots affected by the occasional intrusion of solar stray light.

Section 2 gives an overview of the data and the model system used in the monitoring and section 3 summarizes the results for a one year period taken from the routine monitoring within the operational assimilation system. Section 4 gives examples of the solar stray light effects occurring close to eclipse and during other seasons of the year. The stability of the blackbody calibration is investigated in section 5. Results are summarized in Section 6.

# 2 Data

The monitoring of METEOSAT radiances has been performed operationally since 13 July 1999 within the ECMWF data assimilation system (Munro et al., 1999). It has been extended to provide more detail including monitoring at hourly resolution and the IR channel in 2000 (Köpken, 2001). The monitoring discussed in this report covers the one year period from April 2000 to March 2001.

## 2.1 Clear–sky radiances

The raw WV METEOSAT radiances at their full temporal and spatial resolution represent an enormous data volume and have a very high spatial resolution compared to the resolution currently used for deriving analysis increments (observations at 5 km at sub–satellite point versus analyses at T159, approx. 125 km, resolution). Therefore, the radiances are used at ECMWF in a preprocessed form, the so–called clear–sky radiances (CSR), derived by EUMETSAT for both the WV and IR channel. The CSR represent averages over those pixels of a $16 \cdot 16$ pixel subsegment that are diagnosed as cloud free. Thus, the resolution of the CSR product corresponds to about $80 \cdot 80$ km$^2$ at sub satellite point (SSP) increasing to about $125 \cdot 125$ km$^2$ at $50^o$ from the SSP. Along with the values of CSR and the corresponding brightness temperatures (TB), the percentages of a subsegment that were diagnosed as being cloudy and cloud–free are given. IR radiances are computed only for cloud–free conditions at all levels, while WV radiances are also derived in the presence of low level clouds.

The calibration of the radiometer of MET–5 is a so–called vicarious calibration based on forward radiative transfer calculations. It was developed by EUMETSAT (van de Berg et al., 1995; EUMETSAT, 1996), because the on-board blackbody of the METEOSAT 5 and 6 cannot be used due to mechanical problems. For MET–7 this vicarious calibration has been replaced by a calibration based on its blackbody on 29 May 2000 12:30 UTC (van de Berg, personal communication, briefly discussed in Tjemkes et al., 2001). For MET–5 a cross–calibration with MET–7 using the overlap area of both satellites has been developed and was implemented on 31 May 2001.

The CSR data are received hourly in BUFR format and stored in the ECMWF archive MARS. During the eclipse seasons, one to three slots are excluded from dissemination. The dates and times of excluded slots during the period considered here are listed in Table 1.

### 2.2 Model and assimilation system

The model used in the monitoring at ECMWF is the Integrated Forecasting System (IFS). The versions used here are CY22R3 to CY23R3. The horizontal resolution was increased from T319 to T511 in November 2000 (corresponding to approximately 63 km and 40 km, respectively), the vertical resolution is 60 levels the highest level being at 0.1 hPa. The analysis system is a 4DVAR at initially T63 (320 km) and from November onwards T159 (125 km) horizontal resolution. The assimilation time window was increased from 6 hours to 12 hours in September 2000. The observation monitoring is done in 'measurement space', i.e. for satellite radiances in terms of brightness temperatures (TB). The radiative transfer model used for calculating the model or first guess (FG) TB is RTTOV–5 (Saunders et al., 1999). The dates of model changes taking place within the discussed one year period are listed in Table 2 together with the relevant changed model characteristics. Changes to the CSR observations and periods with missing data are also included.

## 3 Monitoring time series for MET–5 and MET–7

Figure 1 and Figure 2 show the monitoring of the WV–CSR for MET–5 and MET–7, respectively, from April 2000 to March 2001. The time series show the mean departures of the observed radiances from those computed from the model, averaged over the whole disk covered by the satellite (red curves), bias corrected departures (blue curves) and their standard deviation (magenta curve). The time resolution of the monitoring is hourly, i.e. the same as for the incoming data. The mean departures of MET–5, being calibrated using the vicarious calibration method, vary considerably. The range is mostly 2–4 K, but even values of 0.5 K (November 2000, February 2001) and up to 5–5.5 K (April 2000, September 2000), and a short term outlier of 8 K (15 February 2001) occur. The changes often take place over the range of only a few days. During the autumn eclipse season September to October 2000, jumps of more than 2 K even occurred regularly every day. A similar instable behaviour was observed for MET–7 until the introduction of the blackbody calibration on 29 May 2000. The difference is also clearly visible in the operational calibration coefficients displayed in Figure 3. Periods of daily oscillating calibration coefficients for both satellites are visible during the spring eclipse in March and April 2000. Several of the jumps of the calibration coefficient for MET–7 during April and May, e.g. on 18 April and 2, 5, and 7 May, can be clearly associated in time and magnitude to the mean deviations versus the model.

Since the use of the blackbody, the calibration coefficient and the mean departures versus the model remained extremely stable from June 2000 until January 2001. Indeed, this stability even allows to use the Meteosat observations to detect changes in the ECMWF operational system relating to upper tropospheric humidity. This can e.g. be seen in Figure 2 on 29 July 2000 when erroneously warm High Resolution Infrared Sounder Channel 12 (HIRS–12) data were assimilated, causing the MET–7 departures to drop by about 0.4 K. Another event is spotted from 1 to 13 December which is due to a change in the bias correction of the assimilated channel

HIRS–12 (changed back on 13 December) that caused a warming of the model TB's by about 1 K. The regular growth pattern of the standard deviations (magenta line) is associated with the increasing model error with forecast length. Indeed, it shows the transition from a 6–hour to a 12–hour 4DVAR cycle on 12 September 2000 (12 hourly pattern afterwards in contrast to the 6 hourly pattern before).

A small diurnal cycle is visible in the deviations. It is illustrated further in Figure 4 showing statistics separated for land and sea surfaces. It shows that the diurnal variation is only present over land (top panels) while the mean differences over sea are remarkably constant. The diurnal differences occur mostly over convective areas of Africa (see Köpken, 2001). It is believed that they are at least partly caused by the model.

Another striking feature is the regular occurrence of spikes in the time series around local midnight, i.e. 20 UTC for MET–5 and 00 UTC for MET–7. They are growing in magnitude towards the eclipse season, when the worst affected slots are actually excluded by EUMETSAT from dissemination (see Table 1). But some disturbance is present throughout the year, even far from the eclipse period, as is suggested by the small spikes visible around 00 UTC in the mean departures from the model. Examples of the effects causing these are shown in the next section.

# 4 Effects caused by solar stray light

When the satellite 'looks' towards the sun around local midnight and at least a part of the sun is visible behind the northern or southern hemisphere of the earth, solar light may intrude into the radiometer. This is especially the case during the spring and autumn eclipses. Direct sunlight is then reflected and diffused by the mechanical structure of the radiometer and may reach the detectors to create anomalous intense spots and bands. This effect of secondary reflection stray light is present in the visible, but also WV and IR images (EUMETSAT internet page: *http://www.eumetsat.de*). Examples of effects in the water vapour image are shown in Figure 5. The top picture shows the most often occurring effect of very bright (high TB) spots and bows at the top of the image. Another observed effect is a striping pattern of cold TBs at the top of the image which are caused by bright spots being present just outside of the earth disk. This influences the instrument offset of the respective lines which results in lower TBs (van de Berg, personal communication). When effects are severe during the eclipse periods, the images and derived products are not disseminated (see Table 1 for CSR product).

However, more images and CSR products than actually excluded from dissemination are quite severely affected close to the eclipse (April, August 2000, February 2000; see large spikes in mean departures in Figure 2). Also, the monitoring time series indicate that some, though only much smaller, effects are present between the eclipse seasons (see e.g. July and December 2000). Figure 6 illustrates the anomaly that causes such a small spike with an example from 23 December 2000. The top part displays the WV image of 01 UTC, in which no default is obvious. But when looking at the difference between the observations at 01 UTC and 00 UTC (bottom part), a bow appears in the lower part of the image, which is clearly a geometrical and not a natural structure. The amplitude of the effect is 2–4 K. The contrasts in the WV image (top panel) are actually carefully enhanced so that the bow may be distinguished when knowing it is there. But an inspection of the 01 UTC image alone at would not allow normally

to detect it.

To better characterize the times when images are affected and the kind of degradation observed, CSR data of MET–7 for five to ten slots close to midnight have been checked for 20 different dates throughout the year. A selection of the plots is displayed in Figure 7 to Figure 21. For inspecting the data, the same approach as used in Figure 6 has been chosen, i.e. observations from two consecutive hours have been subtracted to more easily detect any degradation. Since the noticed structures do generally not change much from day to day, data from normally three days have been averaged to obtain a better data coverage (CSR data not being available in areas with medium or high level clouds). For comparability of the effects, the same colour scale has been used for all plots although for several severely affected images this scale is insufficient and image parts with strong anomalies appear white (as for missing data). The structure of the differences usually allows to distinguish this from the few areas where no data are available inside the disk in spite of averaging over three days. The obtained difference plots have been compared versus the corresponding departures between observations and first guess. This cross–check confirmed in all but one case that the structures seen in the figures shown are not caused by atmospheric features.

Figure 7 characterizes the situation just at the end of the peak of the spring eclipse period. While the data at 23 UTC seem correct, at 00 UTC the whole upper left half of the image (and hence CSR data) suffers from strong hot spots and warm bows running from the top to the middle left causing the warm anomaly in the difference plot. The amplitude of the effect is up to 30 K. At 01 UTC the upper half is generally too cold (this can be better seen in Figure 22 and is discussed there) and two warm bows appear at the right side. These bows are again visible as negative deviations in the difference 02 UTC minus 01 UTC. The warm difference at the top here results from the already mentioned stronger cold bias in the 01 UTC data. The 02 UTC image itself is also generally calibrated too cold (see difference 03 UTC minus 02 UTC and Figure 22). 03 UTC has an indication of a warm stripe along -30$^o$S.

Figure 8 shows that similar patterns, but already much weaker, are still present around 20 April: warm spots and bows at 00 UTC, including an intense spot off the west coast of south America, cold top of image and warm thin bows at the right side at 01 UTC, too cold image, especially at the top, at 02 UTC.

Beginning of May, in Figure 9, warm bows and image top are still present at 00 UTC, at 01 UTC a cold stripe (of about 1.5–2 K) lies along 10$^o$N and the warm thin bows (about 1.5–2.5 K) are also present at the right hand side.

Mid May, Figure 10, at 00 UTC an intense warm spot is visible over northwest Africa and a 'rest' of the warm bow at the upper left corner. 01 UTC seems to be too cold in the upper part, have a cold stripe along 30$^o$N and the thin bows at the right hand side. 02 UTC has no obvious defaults here (but may be overall slightly too cold as suggested in Figure 22).

In June and July, the data seem generally good with the exception of 01 UTC, where a warm bow at the upper right side crossing at least half of the image persists (Figure 11 and Figure 12; the bow appears broader in Figure 11 since, exceptionally, 8 days are averaged here).

In July a well localised and very bright (warm) spot over Africa appears again (moving westward from day to day) in the 00 UTC data. By beginning of August (Figure 13) it is localized west of north Africa and has a warm anomaly of about 15 K. In 01 UTC a second warm bow on the right side appears again.

Mid August, Figure 14, the warm spot at 00 UTC has reached the south American coast and warm anomalies begin to appear at the upper left side of the image. 01 UTC still has the thinner warm bows. 02 UTC data are on average colder than data at other times of the day (see also Figure 22) and seem to have a colder stripe along the equator.

Just before the autumn eclipse at the end of August, Figure 15, a warm bow is already present at 23 UTC, 00 UTC is severely too warm in the upper left part (up to about 30 K), 01 UTC displays stronger warm bows than during the previous months, and 02 UTC has an anomalously cold upper part.

During September and October the severely affected slots (00, 01, and partly 02 UTC) were not disseminated (Table 1). In the received data, a warm bow can be seen at 23 UTC in the upper and lower left image parts at beginning of September and mid October, respectively (Figure 16 top and bottom part). During November, CSR at 00 UTC and 01 UTC were still excluded from dissemination, 23 UTC seems again without default, as are data at 02 and 03 UTC (Figure 17, top panel).

When on 22 December all data became available again, it could be verified that the 01 UTC slot still displays a warm bow (of about 1–2 K anomaly) in the lower part of the image (Figure 17, bottom panel). This is also present, somewhat stronger, in January (Figure 18, top panel). The strong cold spot in the difference 02 UTC minus 01 UTC in January (bottom panel) off the coast of south America is only weakly present in the departures from the model first guess fields (not shown) and is thus probably not an image anomaly.

Beginning of February a second warm bow appears in the 01 UTC slot (Figure 19) and the 02 UTC data seem generally too cold. By 24 February the lower left part of the image at 00 UTC displays a large warm area and the bows at 01 UTC intensify (Figure 20). In mid–March (Figure 21), during the spring eclipse 2001, a very broad band of too warm TB is diagnosed across $10^o$N to $20^o$S at 03 UTC.

To better discriminate the time slots that may be affected and especially to detect for which periods problems seem to persist, the monitoring time series are displayed in Figure 22 with separate curves for different hours of the day. During June and July 2000 all curves for the slots around midnight (panels on the left) lie closely together and are close to those of not affected slots during the day. In the plot, 06 UTC and 18 UTC are chosen as a reference. But during and closer to the eclipse seasons, the presence of problems may be clearly seen by a spreading of the curves at different hours (e.g. in April 2000, February and March 2001). Looking into more detail, many of the features visible in the examples shown in Figure 7 to Figure 21 can be related to the warm or cold deviation from the 'normal' (06 and 18 UTC in Figure 22) for a certain period. The very small effects of the warm bows in the 01 UTC data with relatively small amplitude of about 2–4 K, are reflected here by slightly but consistently warmer mean departures from the model (green curves in panels on the left). These time series show, as was suggested in the data examples, that this contamination at 01 UTC is present throughout the year. It is detectable in June, July 2000 and again after the prolonged EUMETSAT dissemination stop in December 2000 and January 2001, i.e. even far from eclipse. It grows stronger closer to eclipse in February. Also the weak warm bow occurring at 23 UTC (Figure 16) can be seen in this figure to be present from end of August through to around 20 October (red curve). The strongest warm anomalies occur in the 00 UTC data (see pink curve in April, May, August 2000) which are excluded from dissemination for long periods during

eclipse (Table 1). The cold anomalies occurring in slots after midnight, visible in 01 UTC and 02 UTC in e.g. Figure 7, Figure 8, Figure 13, Figure 14, Figure 15, Figure 19, can actually be more easily spotted in this time series display (yellow line). The cold 02 UTC anomaly occurs from April to nearly end of May 2000, from end of July to around 10 November 2000, and starts again in January 2001. It is maximal in March 2001 with 02 UTC CSR being on average as much as 2.5 K colder than the data of unaffected slots. The time series show that also 03 UTC (green lines, panels on the right side of Figure 22) is affected, though to a lesser degree, at beginning of April 2000, from end of August to end of October 2000 and again in February 2001. Possibly, even 04 UTC is slightly affected in September 2000 and March 2001.

By comparing the behaviour of the slots in these time series to the examples from Figure 7 to Figure 21, one may quite safely associate the deviations to the anomalies caused by the solar stray light. This way of displaying the monitoring time series thus helps to determine the time periods when a certain slot is affected without scrutinizing the data of every day separately. Table 3 gives a summary of the periods for which data from certain hours are affected based on these results. The periods have been chosen to rather 'err on the safe side', i.e. flag data for longer periods if some indication of problems is still visible in Figure 22. The periods and days affected should normally only vary very slightly from year to year (when small changes in the relative positions of satellite, earth, and sun occur; van der Berg, personal communication).

# 5 Stability of blackbody calibration

As discussed above, the stability of the WV–CSR has greatly improved for MET–7 with the introduction of the blackbody calibration. Only recently, since January 2001, smaller changes of 0.5–0.8 K magnitude have occurred (see Figure 2). The change in a coefficient of the blackbody calibration done on 5 January (done to adjust the IR calibration to its level it had before introduction of the blackbody calibration, see Table 2) increased the difference by only about 0.3 K, the rest of the change upwards occurring slowly throughout January and back downwards in February. The reason for this slow drift is not understood currently (van de Berg, personal communication). It may, however, be linked to the eclipse seasons (see below). But in any case, the recent changes are of relatively small magnitude and occur over much longer time scales than the variations seen before the introduction of the blackbody calibration.

To check more closely the stability of the calibration, especially during the eclipse season when the satellite and radiometer experience larger temperature changes during the course of the day, Figure 23 displays the time series of mean departures sampling different times of the day but this time excluding hours that may be affected by the solar stray light. The departures for 5, 6, 9, 16, 19, and 20 UTC are shown with a separate curve for each of these hours. During June, July, and also August 2000 the curves stay very close together and remain stably at 3–3.2 K difference to the model values. During the eclipse season of September/October 2000, first, a small overall cooling of about 0.25–0.4 K can be noted, the bias level of 3 K being regained by mid October. Secondly, the spread between the curves increases. This indicates a slightly less stable calibration level through the course of the day, although the number of blackbody calibrations per day is increased from 1 to 2 and then to 4 during early and main eclipse period. This is done to account for the large changes in temperature that the satellite experiences (van de Berg, personal communication). The increased number of calibration updates per day is also visible in the small steps in the time series in Figure 2 (September 2000 and March 2001).

The higher spread between the curves for different times of day, however, is also observed since December 2000 and then into the current spring eclipse period. Therefore, it is difficult to judge if the effect is really caused by the eclipse itself (e.g. by the cooling of the whole satellite when it enters the earth's shadow).

Overall, the calibration based on the blackbody has led to a stable level of the WV–CSR, although the small changes, as occurring during the autumn eclipse and especially since January 2001 need further observation and studying. As discussed in Köpken (2001), the bias of 3 K is mainly attributed to the calibration of MET–7. Based on published studies (Sohn et al., 2000; Bréon et al., 2000; Tjemkes et al., 2001) and the intercomparison to monitoring results with other satellite instruments (HIRS–12 and channel 3 of the Advanced Microwave Sounding Unit B, AMSU–B) and validation results of RTTOV–5, the bias of WV of MET–7 is currently estimated to be about 2–3 K, the bias for MET–5 possibly slightly larger at 3 K.

# 6 Summary and conclusions

The WV channels of MET–5 and MET–7 are monitored operationally at ECMWF based on the hourly CSR product of EUMETSAT. In the present study, the monitoring results for the one year period April 2000 to March 2001 have been described and discussed. While the radiances of MET–5 are relatively unstable with changes of 2–4 K occurring on very short time scales, sometimes even during one day, MET–7 has been very stable since the introduction of the blackbody calibration. However, a systematic warm bias of about 3 K is diagnosed with respect to the ECMWF model. Most of this deviation is attributed to the calibrations of the satellites, the biases being estimated to be about 3 K for MET–5 and 2–3 K for MET–7. Minor variations of up to 0.5–0.8 K taking place as a slow drift up and down do still occur for MET–7. A small decrease of 0.2–0.4 K of the mean brightness temperatures occurred during the autumn eclipse 2000 and this drift may be linked to eclipse conditions. But the reason for these small changes is not understood currently.

The occurrence of warm and cold anomalies in the WV images (and CSR) for hours around midnight has been investigated in detail. Differencing observations between consecutive hours, it is visible that anomalous effects occur throughout the year. Far from the eclipse season they appear as warm bowed structures, with about 2–4 K amplitude in the 01 UTC data. Closer to eclipse different structures including warm bows, very intense warm spots, anomalously warm and cold horizontal stripes and whole image parts occur. The amplitude of the local warm anomalies may reach 10–30 K close to eclipse, the cold bias over a large part of the image may lead to an average 2.5 K cold bias (mean over the whole disk). While the 01 UTC image is shown to be affected throughout the year (warm bows), 23 UTC, 00 UTC and 02 UTC, 03 UTC and possibly also 04 UTC are affected with anomalies of different strength. In several time slots, the anomalies occur for considerable periods before and after the spring and autumn eclipses.

The parts of the image that are affected vary with season, i.e. with the position of the satellite relative to the earth and the sun. The position and occurrence of the effects may thus vary very slightly between years due to small changes in the orbit of the satellite, e.g. due to satellite manoeuvres, (van de Berg, personal communication). Clearly, such data contamination has to be taken into account when using the WV radiances for quantitative evaluations, e.g.

in radiance assimilation or for retrievals of upper tropospheric humidity (UTH). Based on the plots sampled throughout the year and the monitoring time series shown, the periods and times of day during which images are affected may be better diagnosed and excluded. But since mostly only a part of the image is contaminated, an a–priori exclusion of data only in affected areas, or better, a flagging of those data, would be preferable. Since the phenomenon occurs at a special constellation of the sun, the earth, and the optics of the radiometer, the question arises, whether a prediction of the effects based on a geometrical approach may be feasible. An automatic flagging of data contaminated by solar stray light as well as a further clarification of the absolute calibration of the MVIRI, for WV possibly through cross-calibration versus other humidity sounding channels, would further enhance the value of the MVIRI WV channel for quantitative use.

**Acknowledgements.** I would like to thank Leo van de Berg and Marie Doutriaux–Boucher (both from EUMETSAT) for their time spent in discussions and email exchanges on the effects diagnosed in the monitoring at ECMWF. Leo van de Berg provided information on the eclipse problem and known image deficiencies.

## References

Bréon, F.-M., Jackson, D. L., 2000: Calibration of the Meteosat water vapour channel using collocated NOAA/HIRS 12 measurements. *J. of Geophys.Res.*, 105, 11925–11933.

EUMETSAT, 1996: MTP MPEF Algorithm Specification Document, EUM MTP SPE 030 and Appendix A. Available from EUMETSAT. (http://www.eumetsat.de/, go to Data, Products and Services, then Meteorological Product Extraction, then Documentation.)

Köpken, C., 2001: Monitoring and assimilation of Meteosat radiances within the 4DVAR system at ECMWF. *EUMETSAT/ECMWF Fellowship Report No. 9.*

Munro, R., Kelly, G., Saunders, R., 1999: Assimilation of METEOSAT Radiance Data within the 4DVAR system at ECMWF. *EUMETSAT/ECMWF Fellowship Report No. 8.*

Saunders, R. W., M. Matricardi, and P. Brunel, 1999: An improved fast radiative transfer model for assimilation of satellite radiance observations. *Quart. J. Roy. Meteor. Soc.*, 125, 1407–1425.

Sohn, B. J., Schmetz, J., Tjemkes, S., Koenig, M., Lutz, H., Arriaga, A., Chung, E. S., 2000: Intercalibration of the METEOSAT–7 water vapour channel with SSM/T–2. *J. of Geophys. Res.*, 105, 15673–15680.

Tjemkes, S., and J. Schmetz, 1997: Synthetic satellite radiances using the radiance sampling method. *J. Geophys. Res.*, 102, 1807–1818.

Tjemkes, S. A., König, M., Lutz, H.-J., van de Berg, L., 2001: Calibration of Meteosat Water Vapour Channel observations with independent observations. *J. of Geophys.Res.*, 106, 5199–5209.

van de Berg, L. Schmetz, J., Whitlock, J., 1995: On the calibration of the Meteosat water vapour channel. *J. of Geophys.Res.*, 100, 21069–21076.

Table 1: Periods for which CSR data of certain hours were not disseminated by EUMETSAT during spring and autumn eclipse seasons (and longer in case of detected remaining solar stray light effects) in the year investigated here from April 2000 to March 2001.

| | No CSR Disseminated | | |
|---|---|---|---|
| CSR slot | Spring Eclipse | | Autumn Eclipse |
| MET–7 | 2001 | 2000 | 2000 |
| 00 UTC | 27/02 – 31/03 | 01/04 – 11/04 | 01/09 – 29/11 |
| 01 UTC | 01/03 – 31/03 | 01/04 – 05/04 | 01/09 – 21/12 |
| 02 UTC | – | – | 01/09 – 16/10 |
| MET–5 | 2001 | 2000 | 2000 |
| 20 UTC | 15/02 – 31/03 | 01/04 – 03/04 | 19/08 – 06/10 |
| 21 UTC | 23/02 – 17/03 | – | 21/08 – 05/10 |
| 22 UTC | – | – | 21/08 – 05/10 |

Table 2: Summary of changes and special events occurring in the operational assimilation system and CSR observations which are relevant to the monitoring during the period April 2000 to March 2001. 'M' and 'O' indicate changes in the model (ECMWF) and observations (EUMETSAT), respectively.

| Date | | Change |
|---|---|---|
| 1 April – 27 June 2000 | M | Monitoring results shown are from CY22R3 (experimental suite 5011): Horizontal resolution is T319/T63, i.e. $\approx$ 60 km/320 km for the model/derivation of analysis increments; 60 vertical levels. HIRS–12 data used actively. |
| 25–29 May 2000 | M | Exclusion of METEOSAT data from passive processing at ECMWF |
| 29 May 2000, 12:30 UTC | O | Introduction of blackbody calibration for MET–7 |
| 27 June 2000, 00 UTC | M | ECMWF CY22R3: Operational use of HIRS–12 data (and other changes) |
| 29 July 2000 | M | Occurrence of erroneously high radiances from HIRS–12 on NOAA 15 |
| 12 September 2000 | M | ECMWF CY23R1: Introduction of 12 hour 4DVAR (and other changes) |
| 12–17 September 2000 | M | No monitoring due to CSR data processing problem at ECMWF |
| 8 November 2000 | M | Change of the bias correction applied to HIRS–12 |
| 21 November 2000 | M | ECMWF CY23R3: Model resolution increased to T511/T159, i.e. $\approx$ 40 km/125 km for the model/ derivation of analysis increments; 60 vertical levels. |
| 13 December 2000 | M | Correction of erroneous HIRS–12 bias correction and retuned bias correction for METEOSAT 5 and 7 |
| 5 January 2001 | O | Change in the blackbody calibration of METEOSAT 7 to adjust the calibration of the IR channel. The change should increase WV brightness temperatures by about 0.8 degrees. |

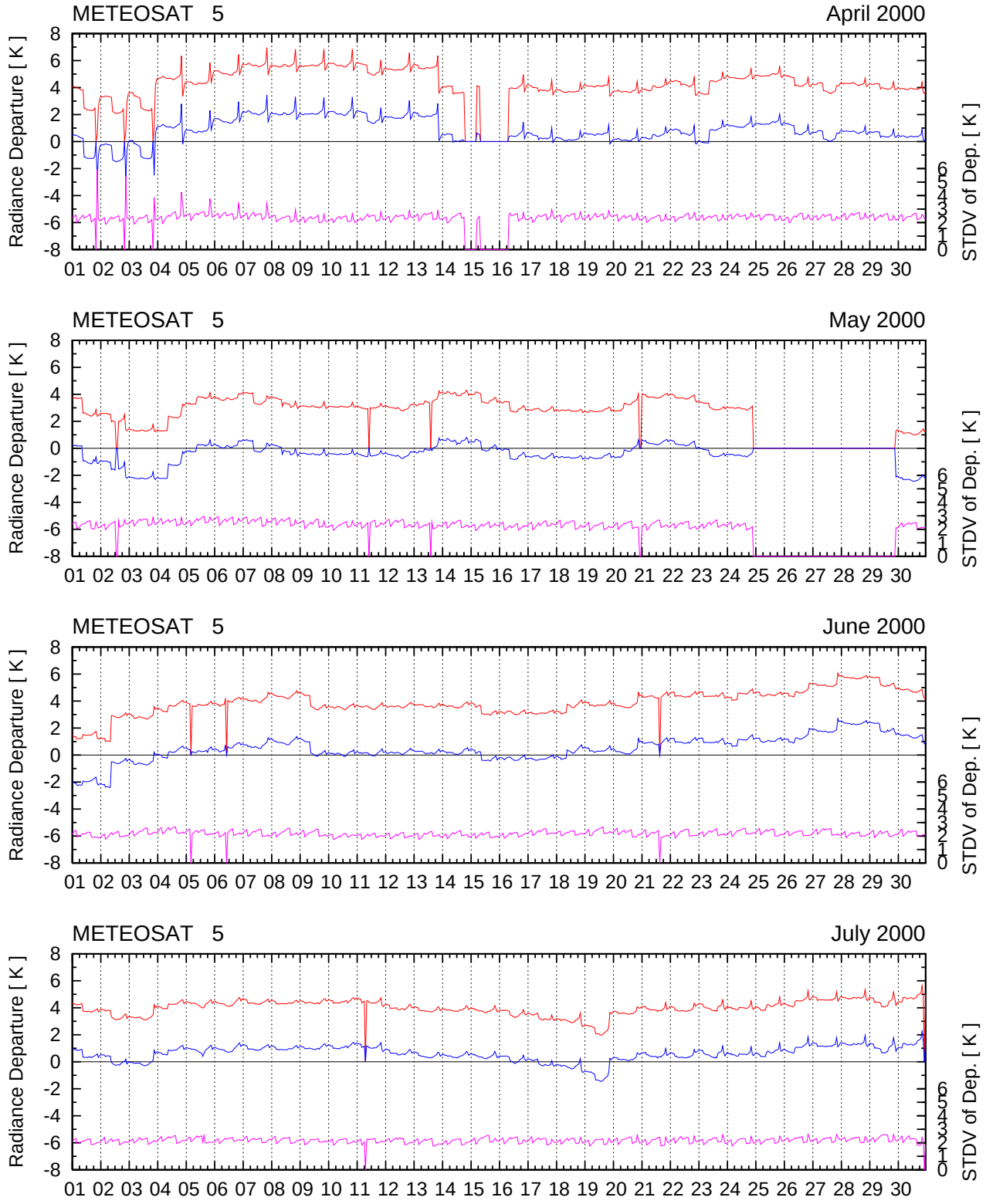


Figure 1: Time series of differences in WV clear–sky radiances from METEOSAT–5 and the corresponding forward calculations from ECMWF model FG for April 2000 to March 2001 (expressed as brightness temperature, TB, difference in K). Curves show the mean TB difference over the whole disk (red line), the bias corrected mean difference (blue line), and standard deviation of differences (magenta line, scale on the right); curves drop to zero if no data are available. For changes in the model and observations, see Table 2.

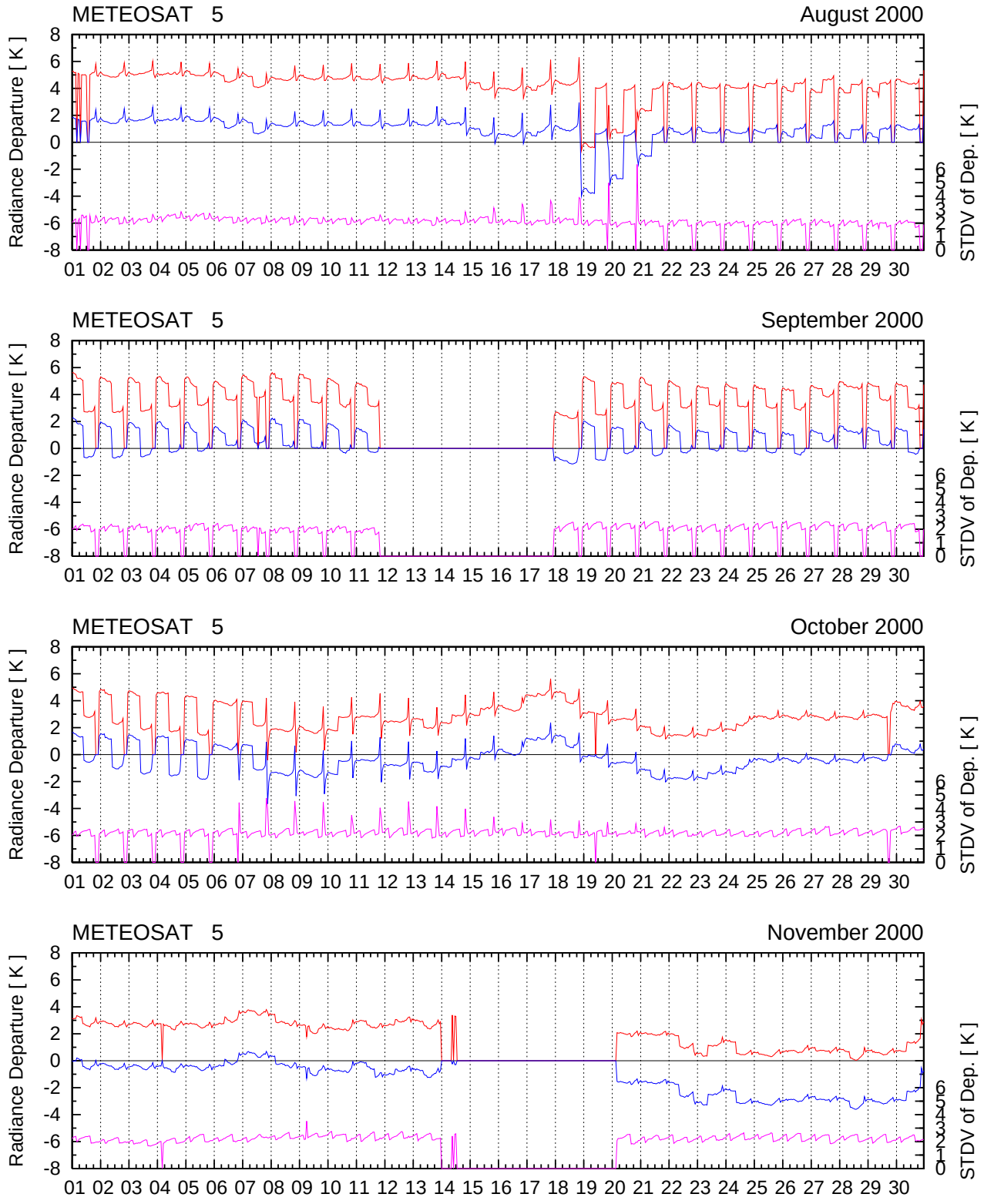


Figure 1: Continued.

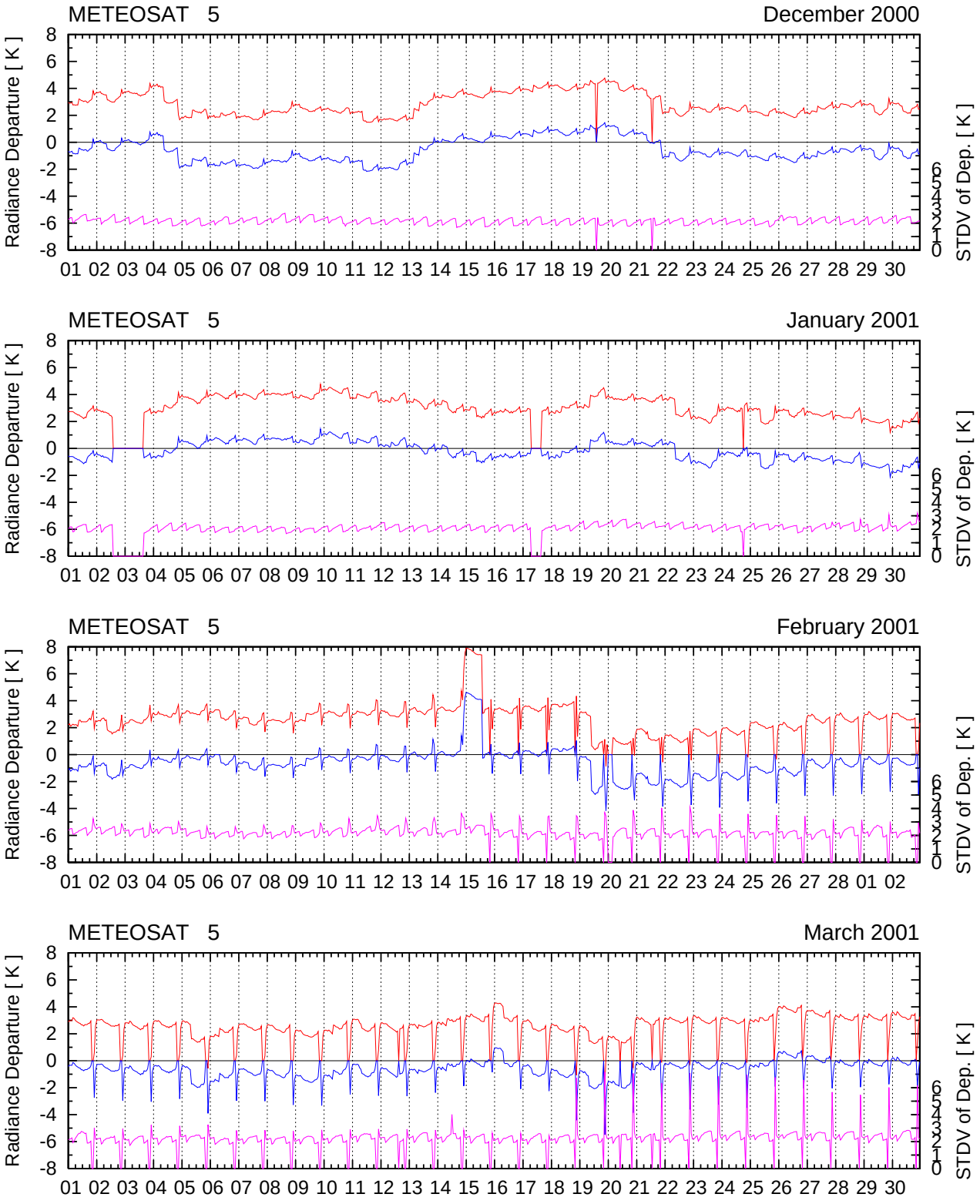


Figure 1: Continued.

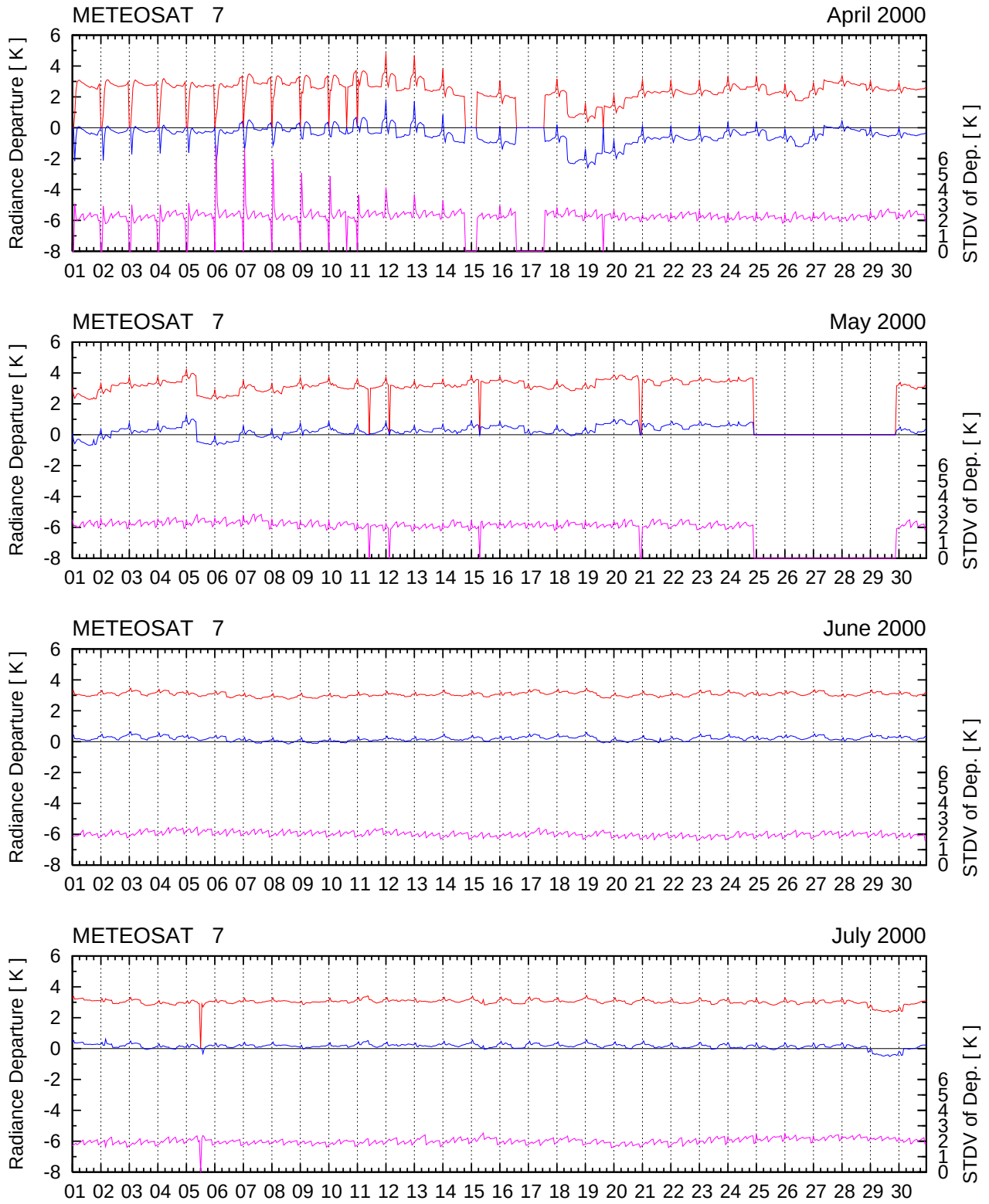


Figure 2: Time series of differences in WV clear–sky radiances from METEOSAT–7 and the corresponding forward calculations from ECMWF model FG for April 2000 to March 2001 (expressed as brightness temperature, TB, difference in K). Curves show the mean TB difference over whole disk (red line), the bias corrected mean difference (blue line), and standard deviation of differences (magenta line, scale on the right); curves drop to zero if no data are available. For changes in the model and observations, see Table 2.

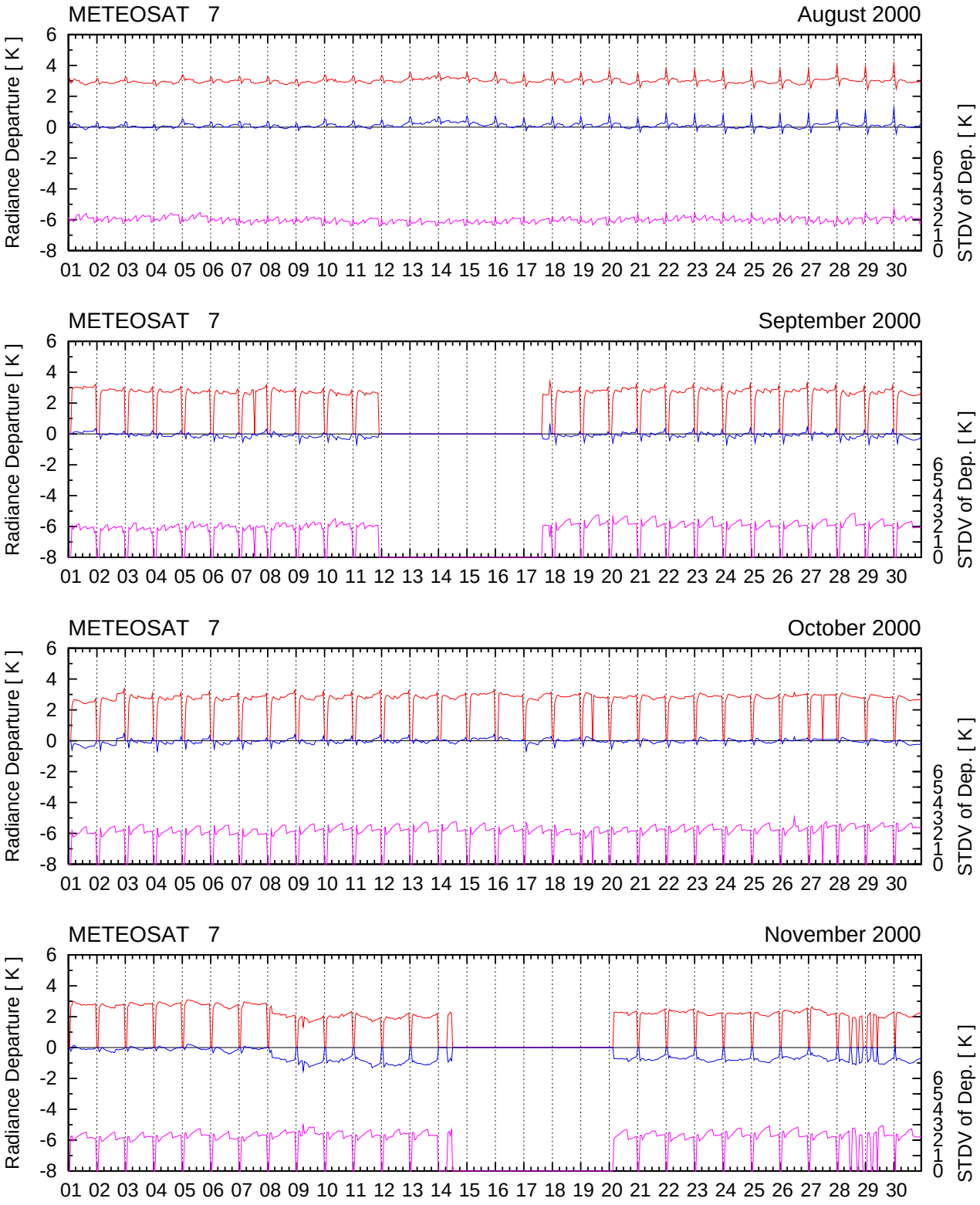


Figure 2: Continued.

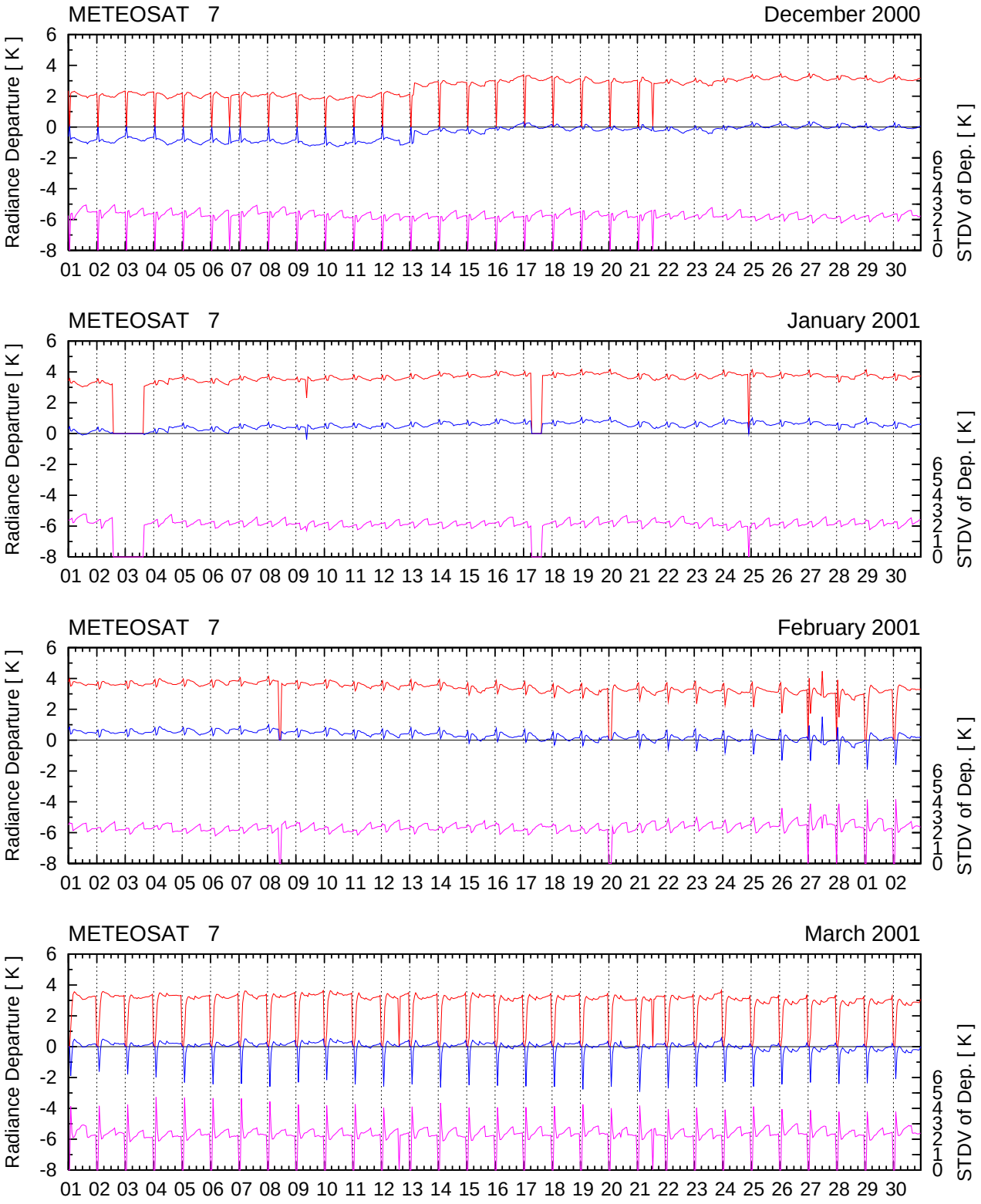


Figure 2: Continued.

METEOSAT Calibration Coefficients : Water Vapour Channel

$$R = \alpha \cdot (C - C_0)$$

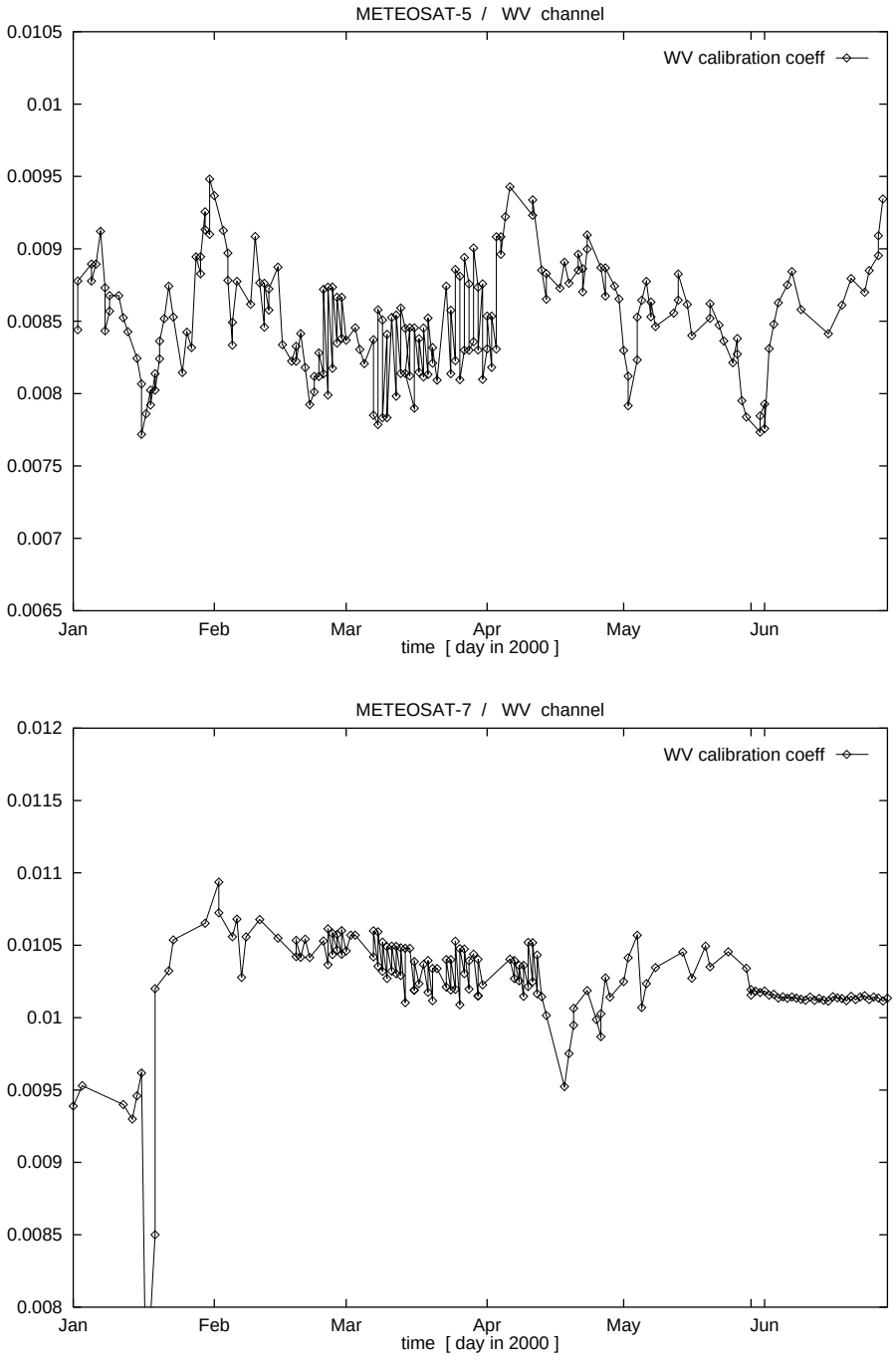


Figure 3: Time series of the operational calibration coefficients ($\alpha$) for the WV channels of MET–5 (top) and MET–7 (bottom). On 29 May 2000 a blackbody calibration replaced the vicarious calibration for MET–7. C is the satellite count, $C_o$=6 the fixed space count, R the resulting radiance. Data are taken from *http://www.eumetsat.de.*

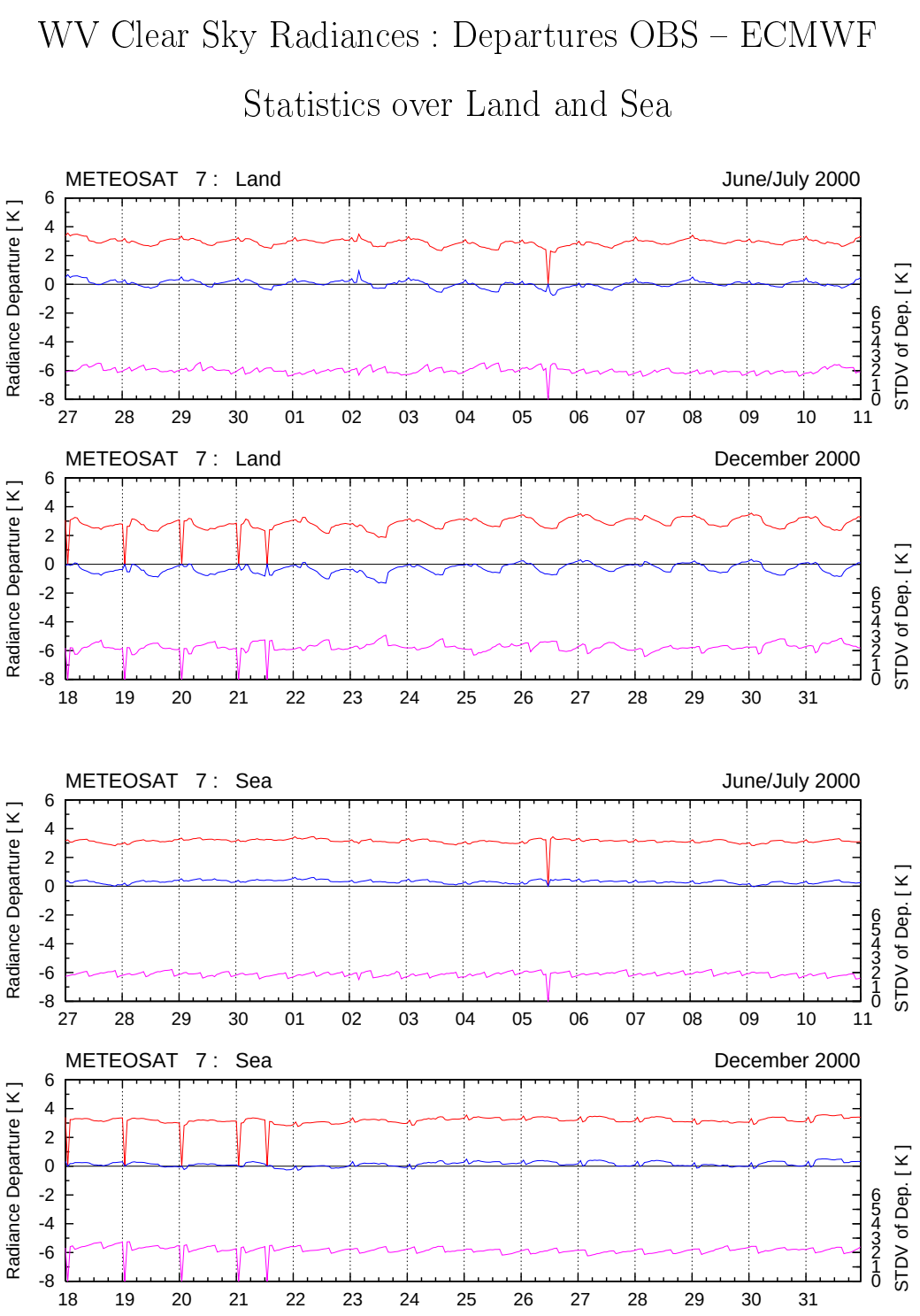


Figure 4: Time series of differences between WV–CSR and ECMWF FG separated for land (top two panels) and sea areas (bottom two panels) of the MET–7 disk. Example for periods in June/July and December 2000. Representation as in Figure 2.

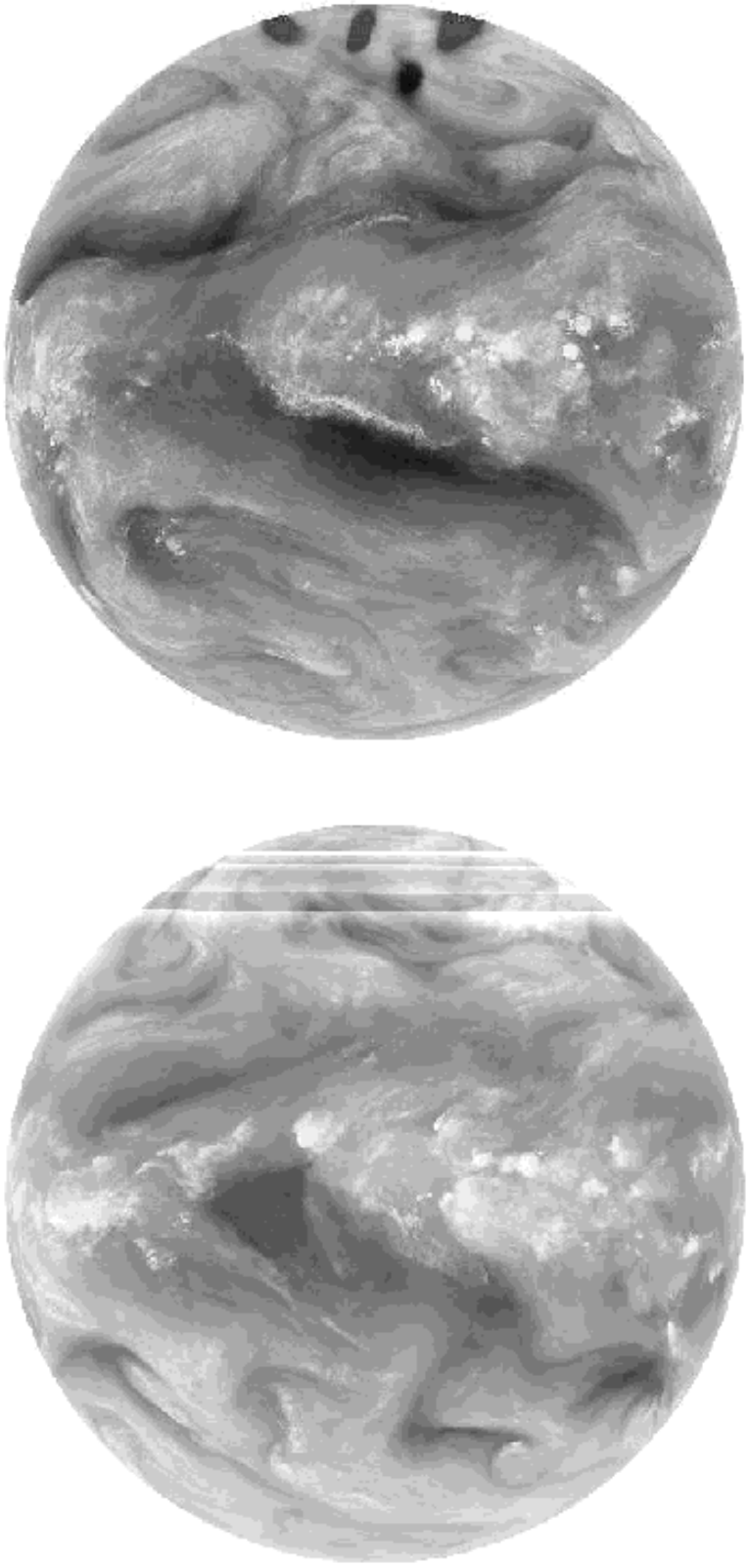

Figure 5: Top: Example of dark spots and bow shaped structures of anomalously high TB in a WV image at midnight. Bottom: Example of pattern of cold stripes at top of WV image. Images taken from EUMETSAT internet page *http://www.eumetsat.de.*

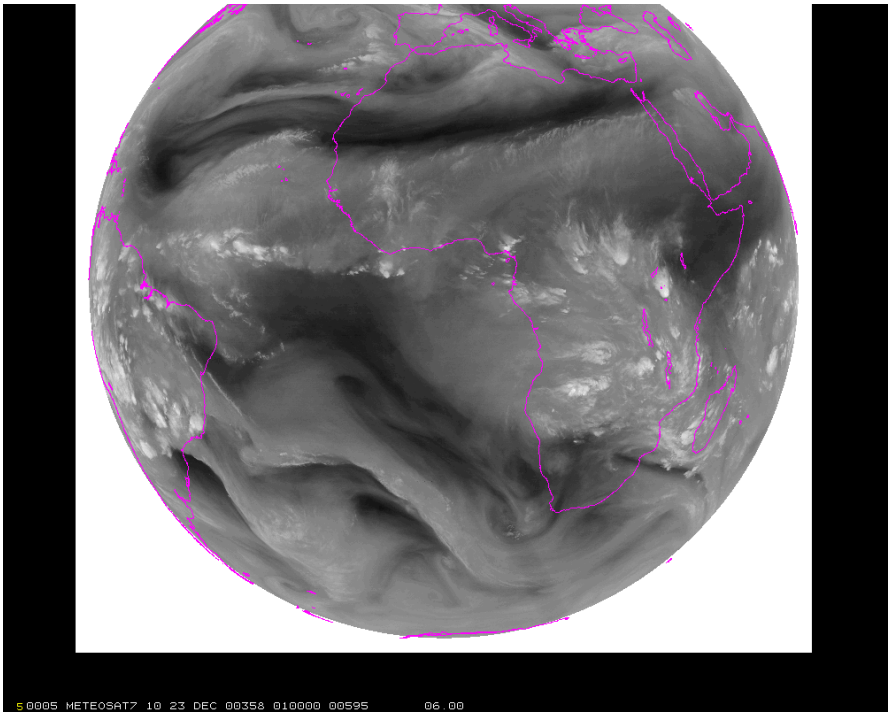


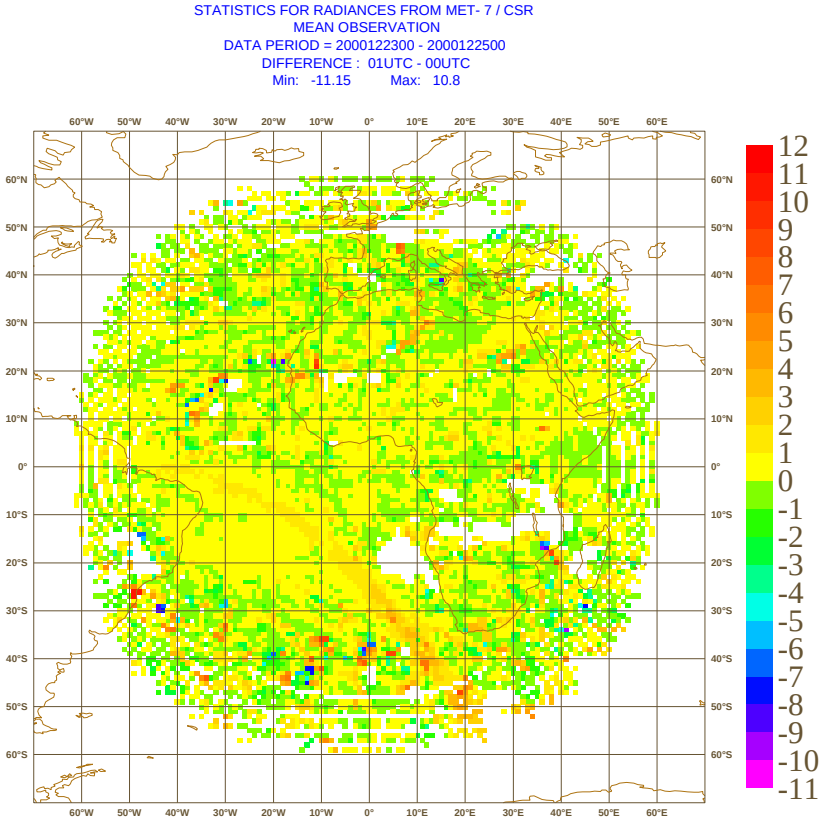


Figure 6: Top: MET–7 WV image of 01 UTC 23 December 2000 (from ECMWF archive). Bottom: Difference between the WV–CSR observations at 1 UTC and 0 UTC (in K). Data are averaged from 23 to 25 December 2000 to achieve a more continuous data coverage since no CSR are available in areas with medium or high level clouds.

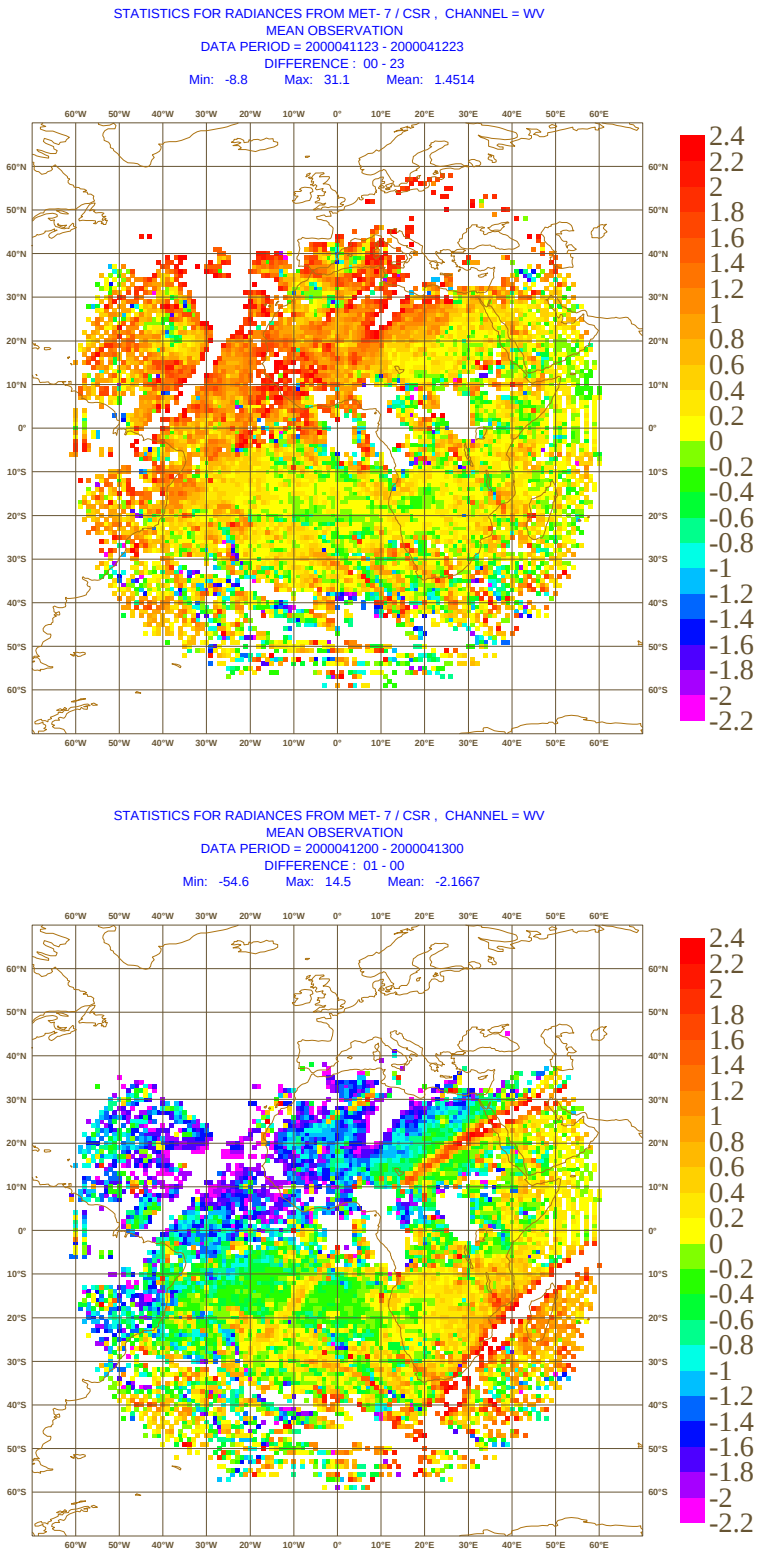


Figure 7: Difference between the WV–CSR observations of two consecutive hours (as brightness temperature in K). Data are averaged over 3 days, here 12–13 April 2000, to achieve a more continuous data coverage since no CSR are available in areas with medium level or high clouds. Top: 00 UTC minus 23 UTC of previous day. Bottom: 01 UTC minus 00 UTC. Note that differences in some anomalies, their maximum being about 30 K at the top of the image, exceed the colour scale. These areas appear white.

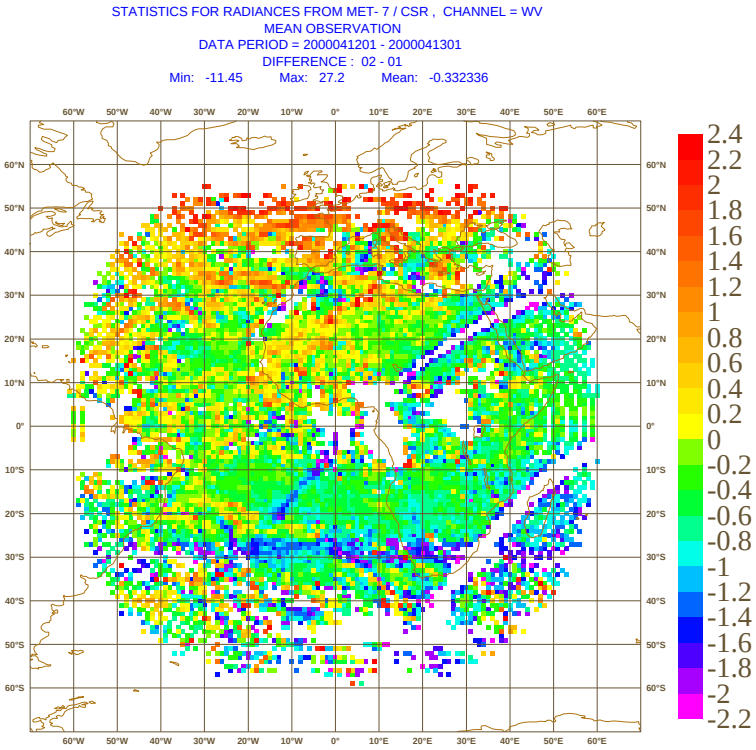


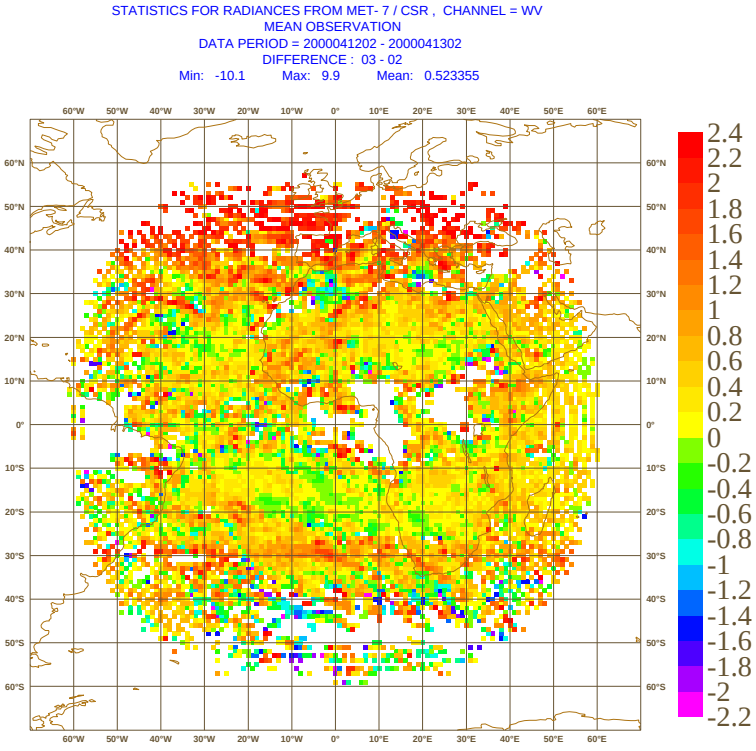


Figure 7: Continued. Top: 02 UTC minus 01 UTC. Bottom: 03 UTC minus 02 UTC.

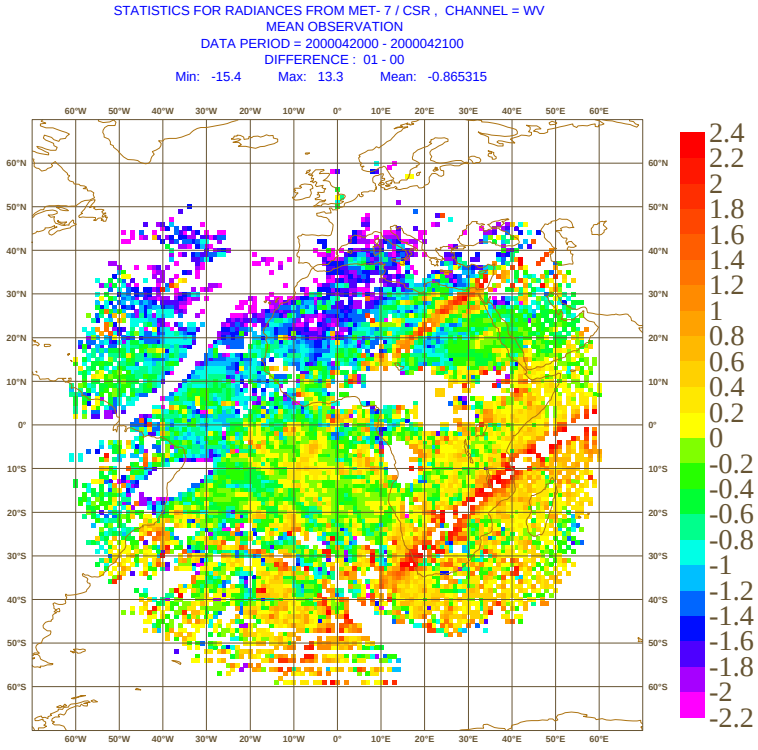


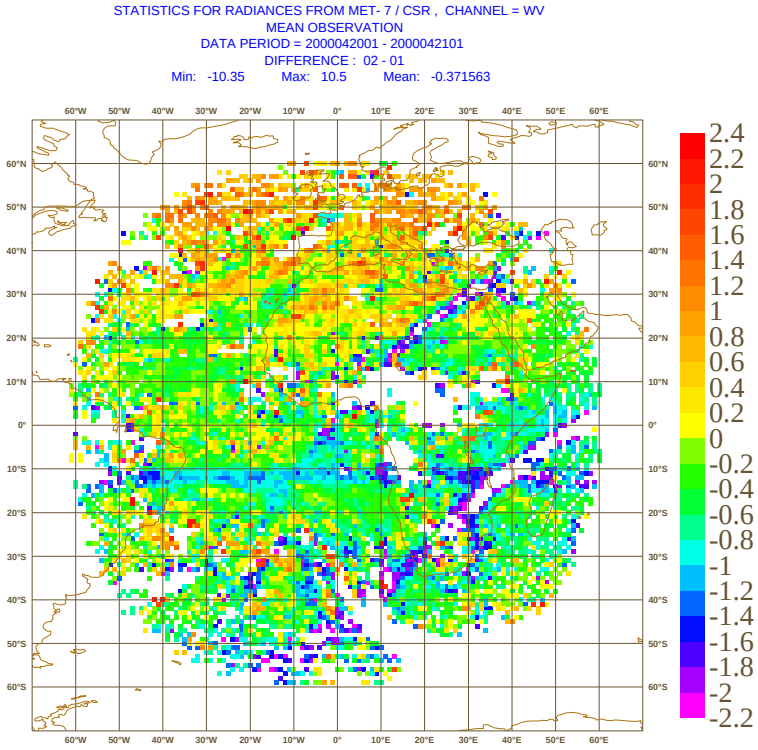


Figure 8: As Figure 7 but for 20–21 April 2000. Top: 01 UTC minus 00 UTC. Bottom: 02 UTC minus 01 UTC. (Note that differences in some anomalies exceed the colour scale, those areas appear white).

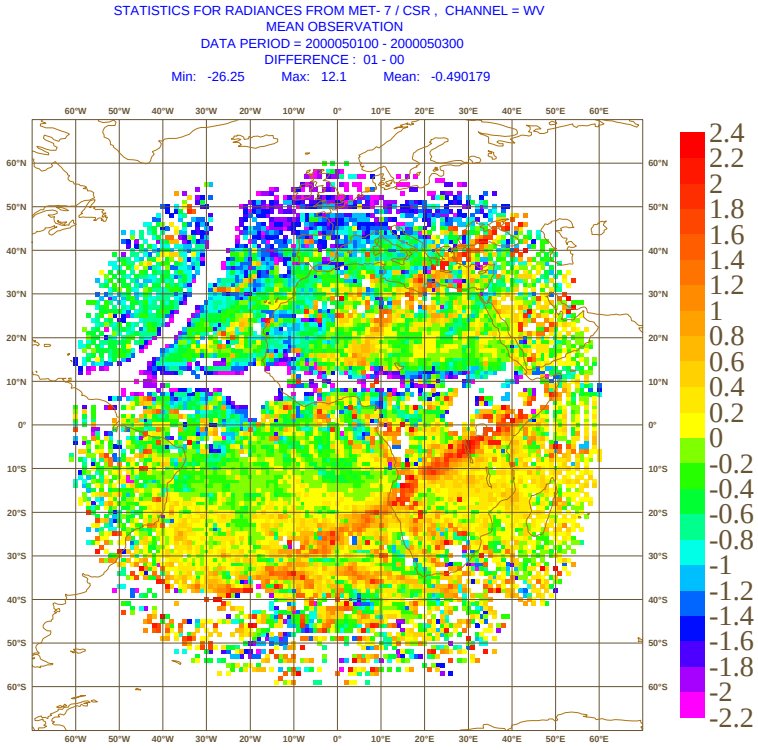


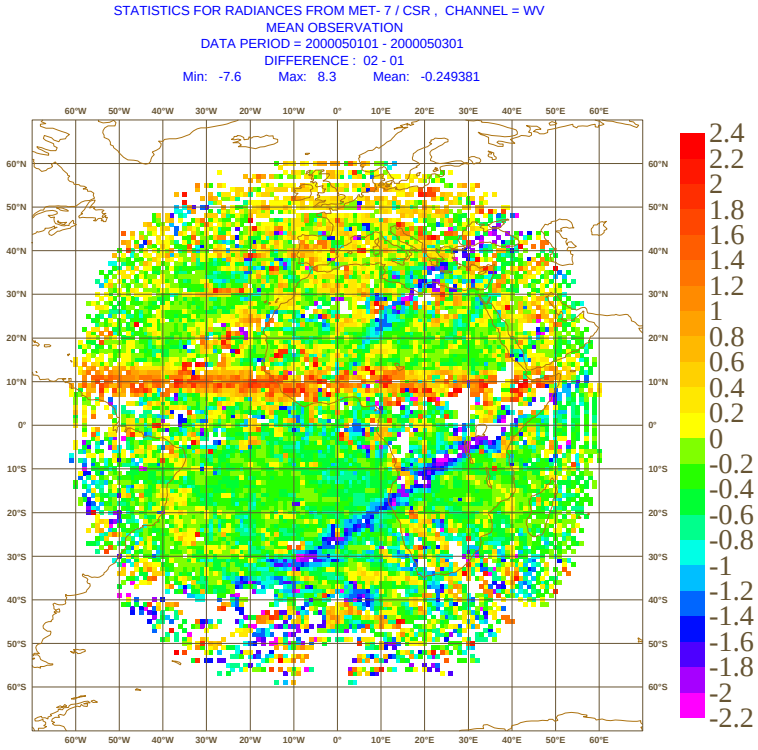


Figure 9: As Figure 7 but for 1–3 May 2000. Top: 01 UTC minus 00 UTC. Bottom: 02 UTC minus 01 UTC. (Note that differences in some anomalies exceed the colour scale, those areas appear white).

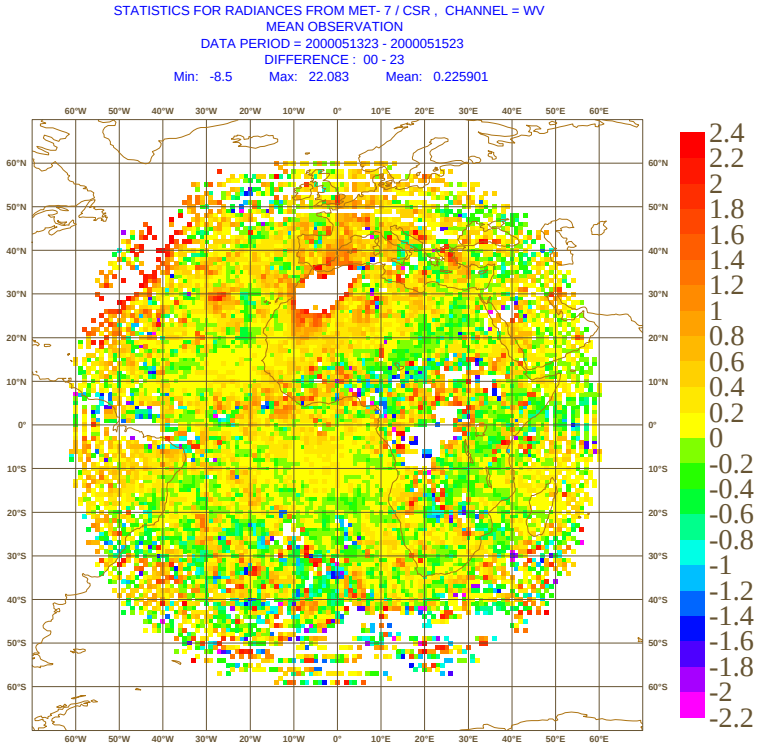


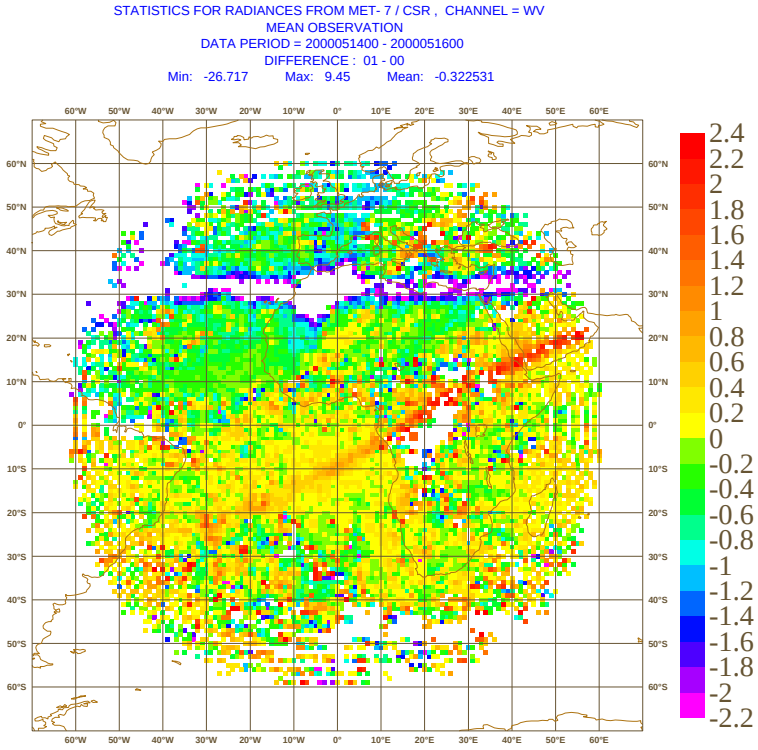


Figure 10: As Figure 7 but for 14–16 May 2000. Top: 00 UTC minus 23 UTC of previous day. Bottom: 01 UTC minus 00 UTC. (Note that differences in some anomalies exceed the colour scale, those areas appear white).

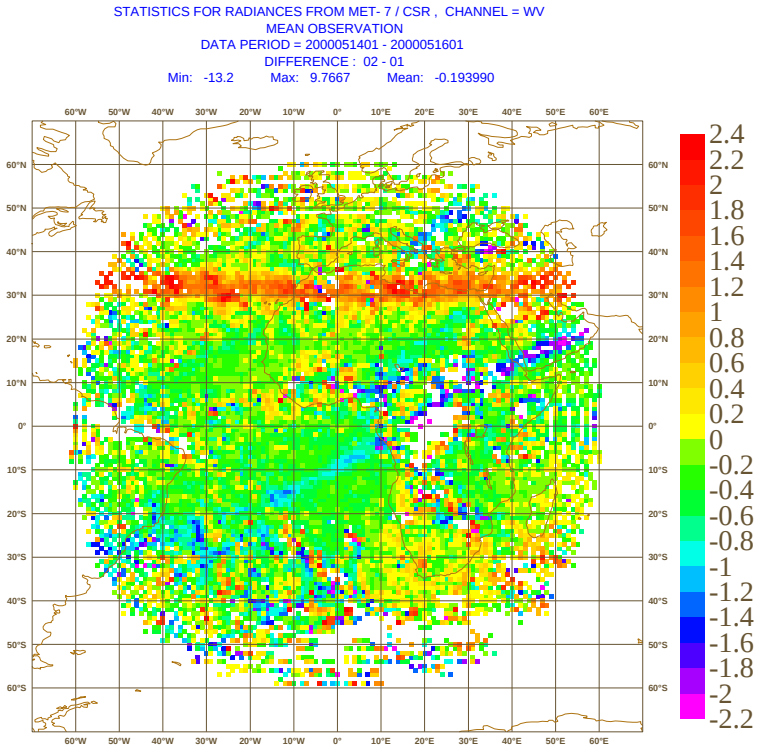


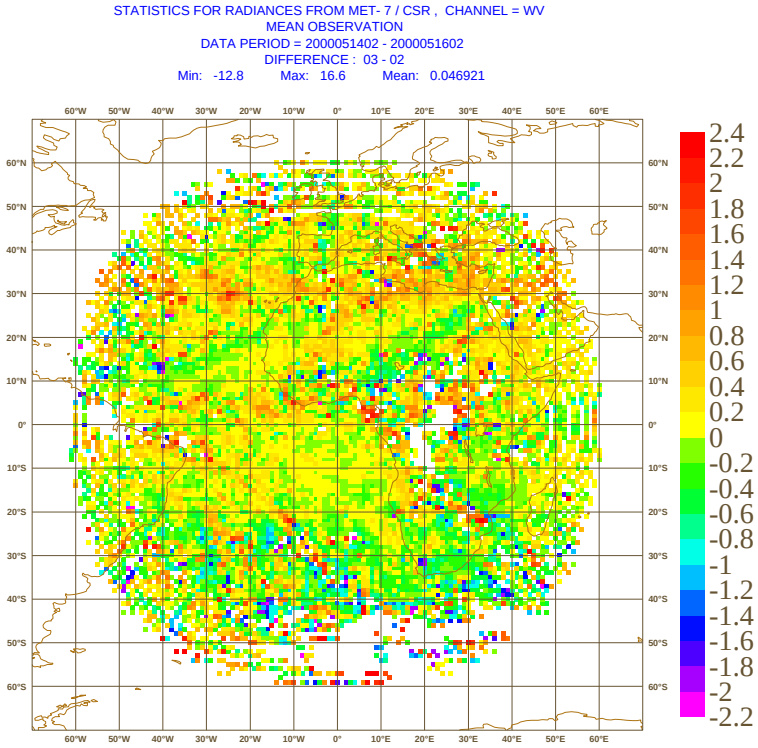


Figure 10: Continued. Top: 02 UTC minus 01 UTC. Bottom: 03 UTC minus 02 UTC.

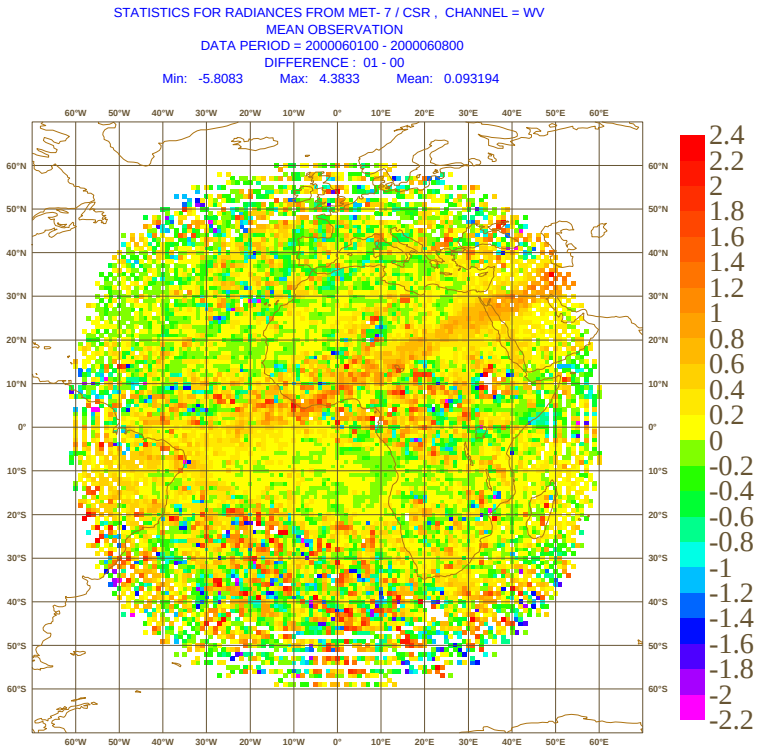


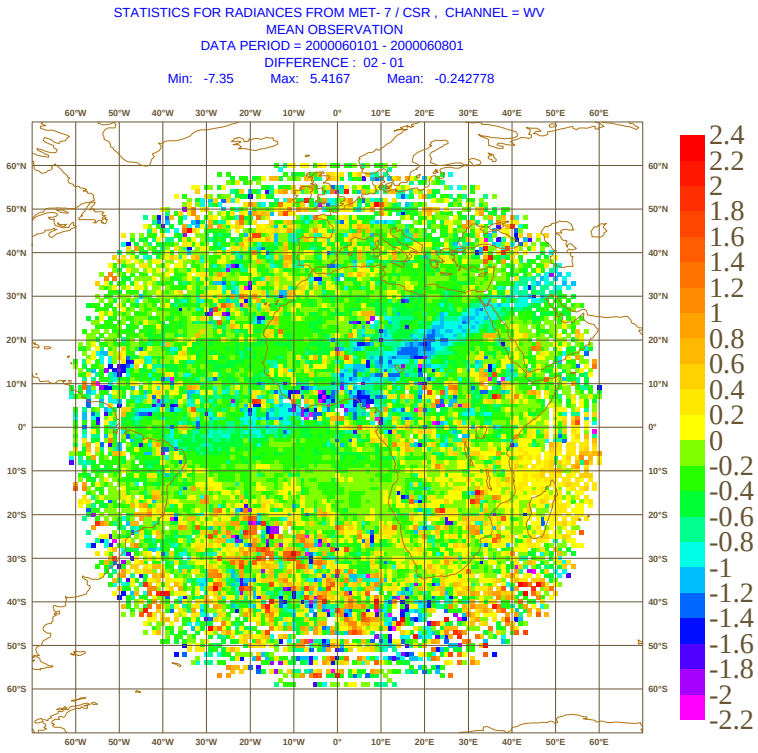


Figure 11: As Figure 7 but for 1–8 June 2000. Top: 01 UTC minus 00 UTC. Bottom: 02 UTC minus 01 UTC.

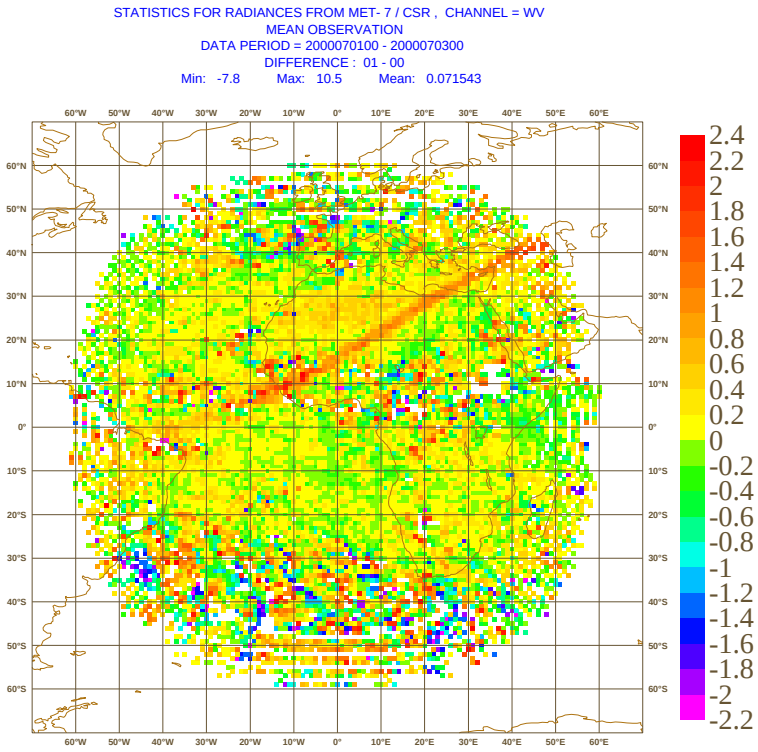


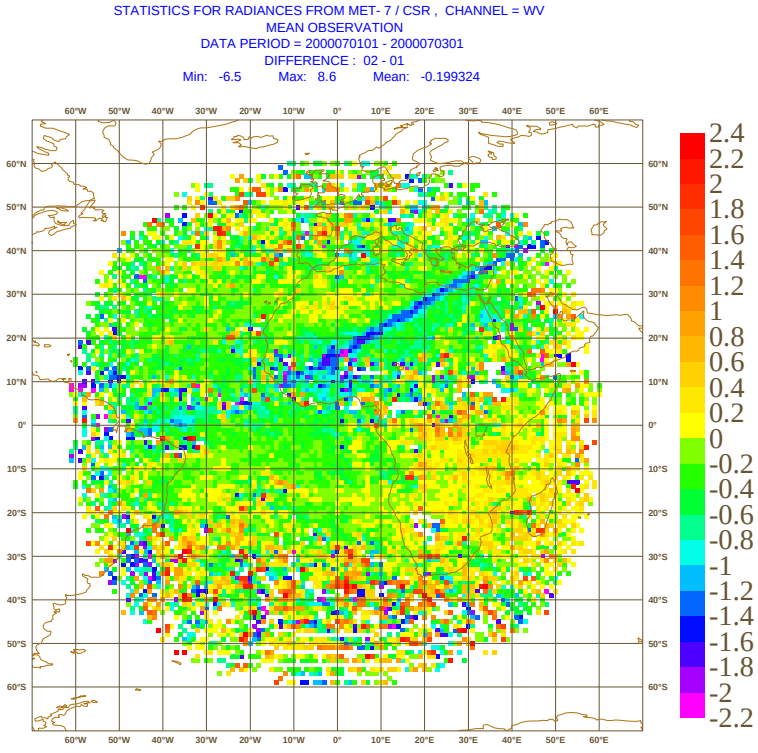


Figure 12: As Figure 7 but for 1–3 July 2000. Top: 01 UTC minus 00 UTC. Bottom: 02 UTC minus 01 UTC.

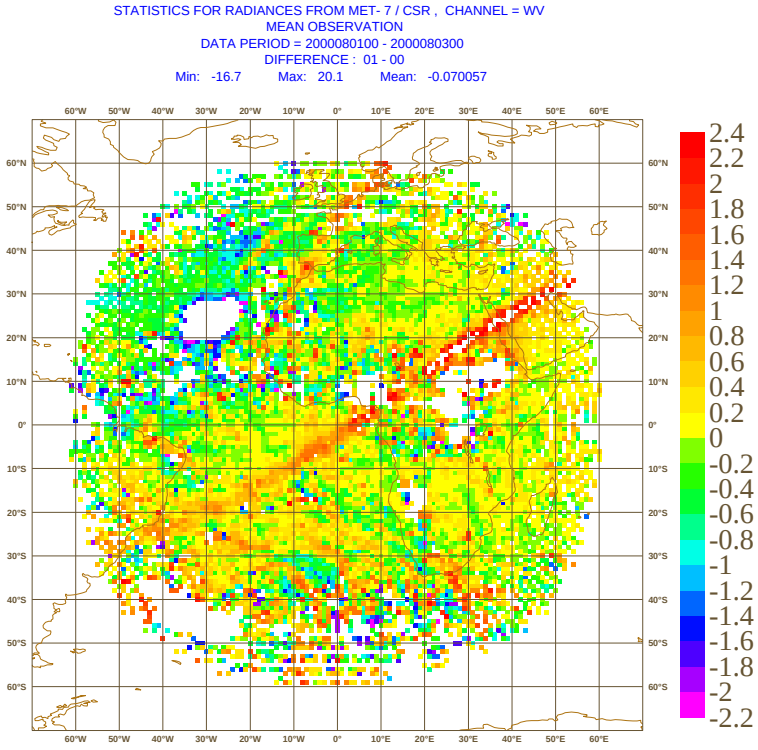


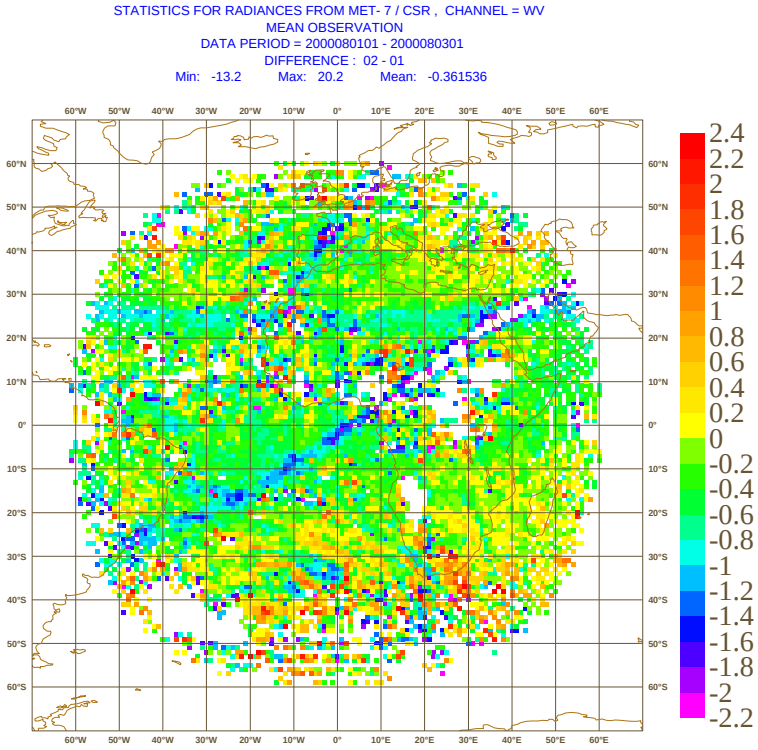


Figure 13: As Figure 7 but for 1–3 August 2000. Top: 01 UTC minus 00 UTC. Bottom: 02 UTC minus 01 UTC. (Note that differences in some anomalies exceed the colour scale, those areas appear white).

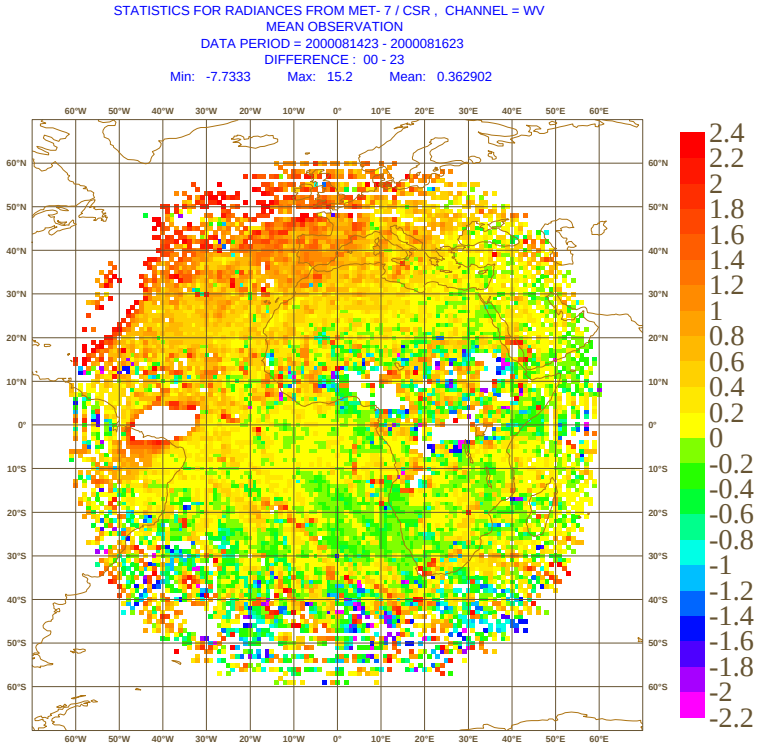


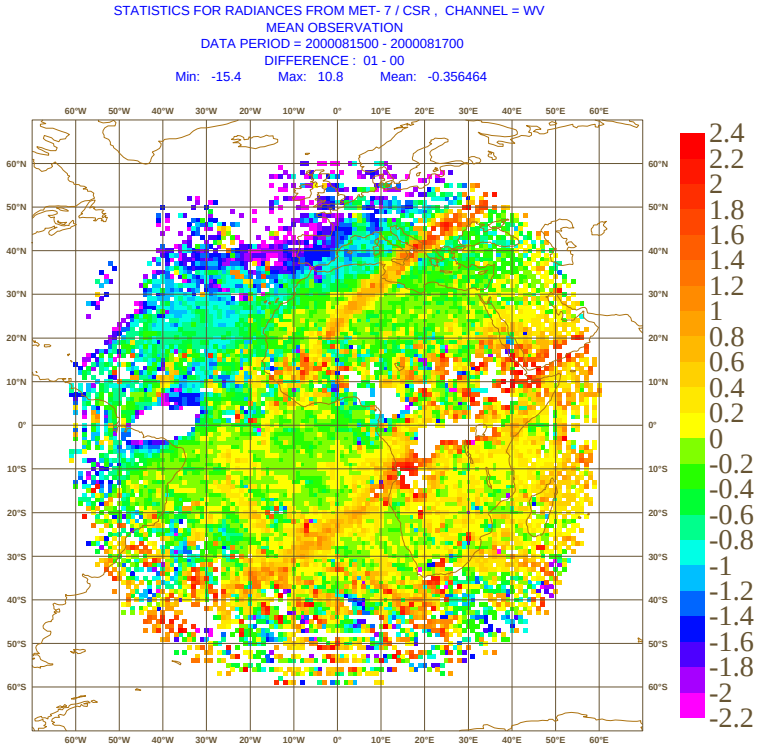


Figure 14: As Figure 7 but for 15–17 August 2000. Top: 00 UTC minus 23 UTC of previous day. Bottom: 01 UTC minus 00 UTC. (Note that differences in some anomalies exceed the colour scale, those areas appear white).

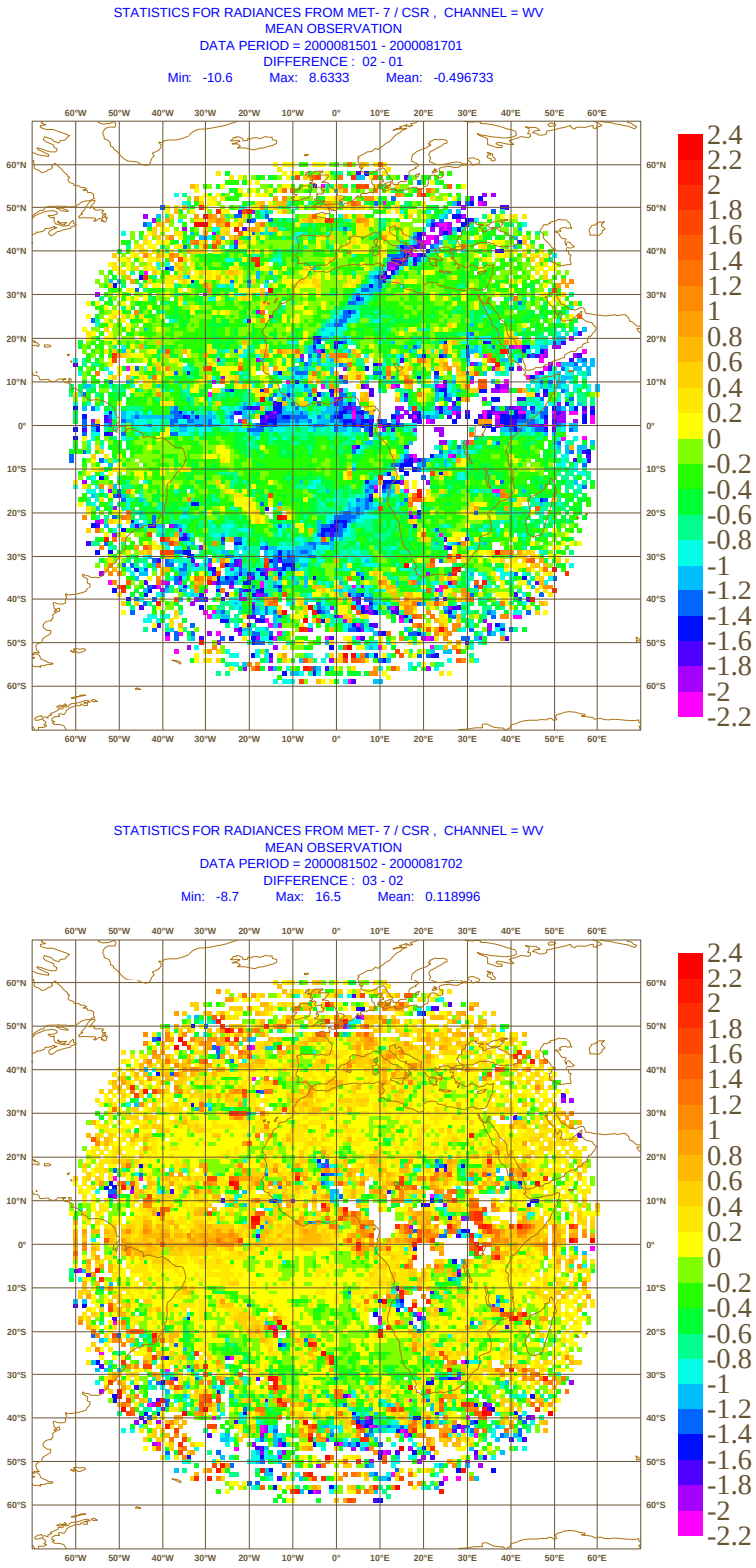


Figure 14: Continued. Top: 02 minus 01 UTC. Bottom: 03 UTC minus 02 UTC.

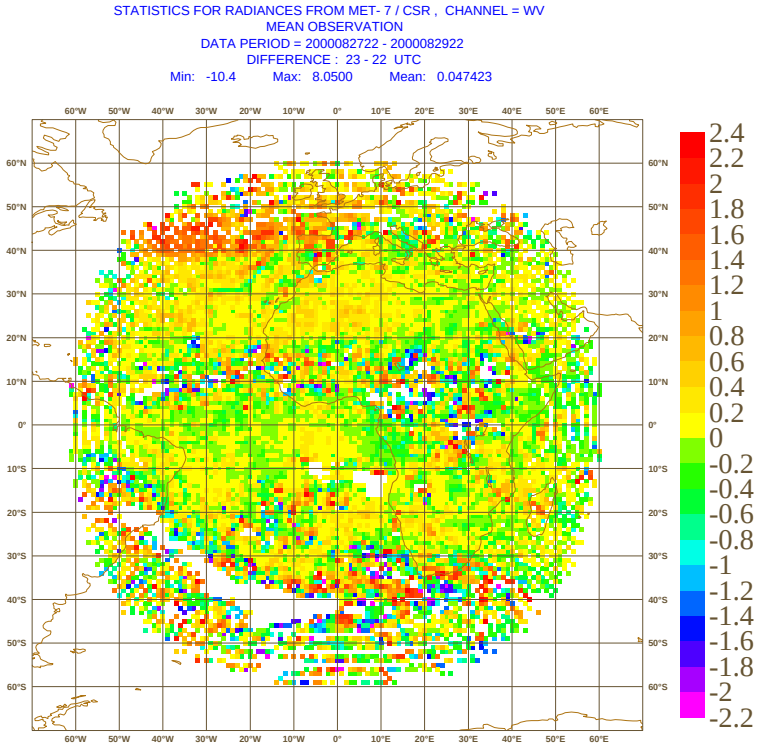


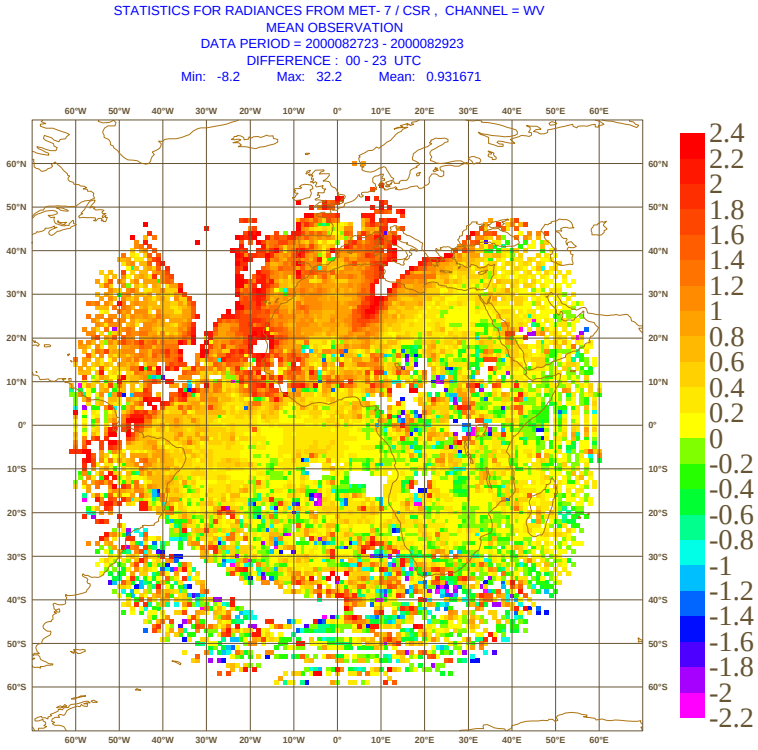


Figure 15: As Figure 7 but for 28–30 August 2000. Top: 23 UTC minus 22 UTC. Bottom: 00 UTC minus 23 UTC of previous day. (Note that differences in some anomalies exceed the colour scale, those areas appear white).

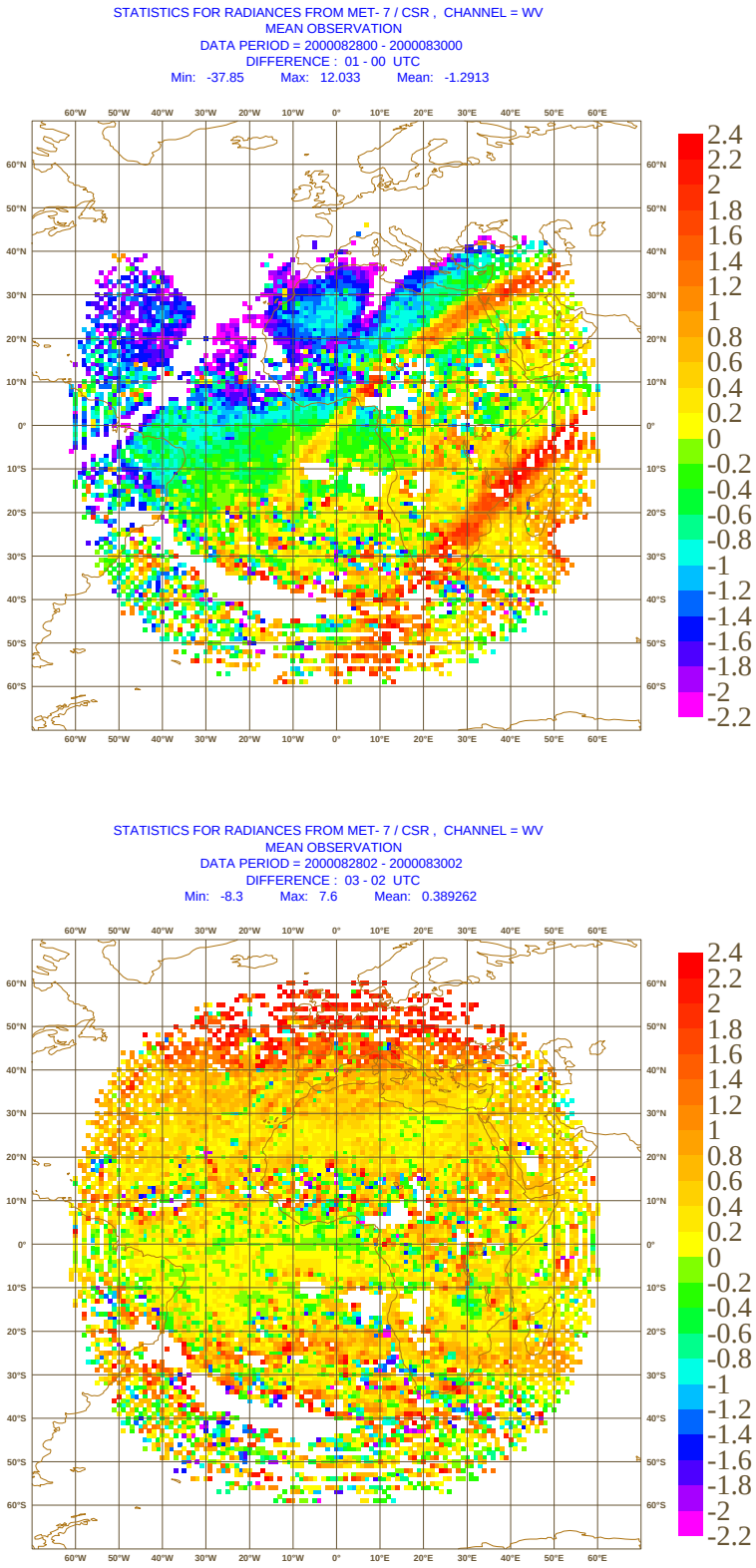


Figure 15: Continued. Top: 01 UTC minus 00 UTC. Bottom: 03 UTC minus 02 UTC.

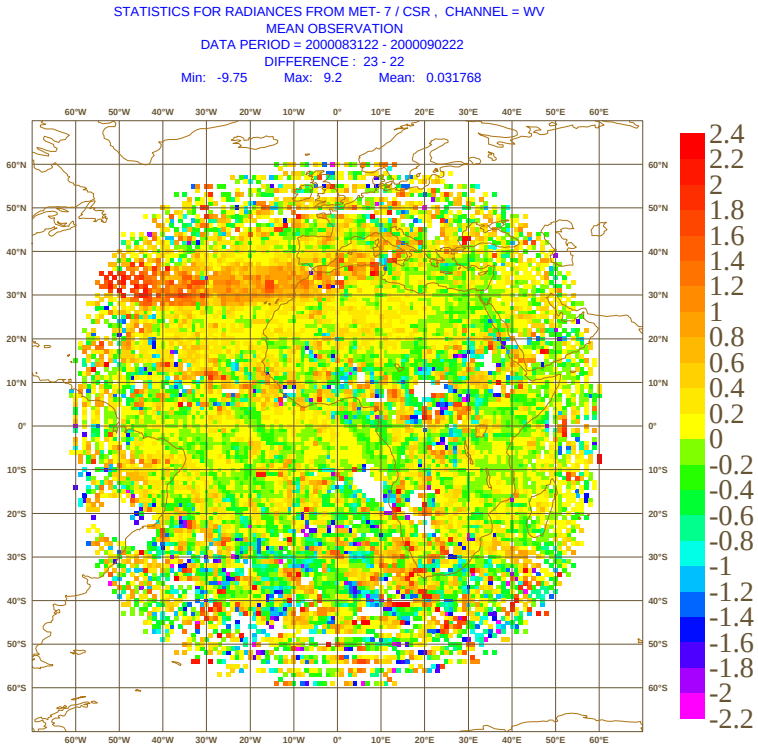


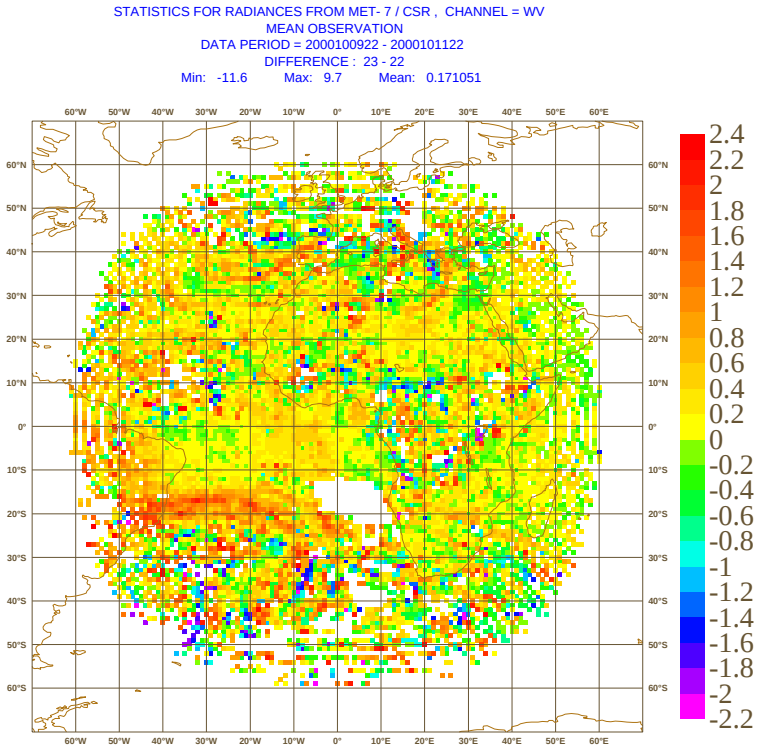


Figure 16: As Figure 7 but for: Top: 31 August – 2 September 2000, 23 UTC minus 22 UTC. Bottom: 9–11 October 2000, 23 UTC minus 22 UTC.

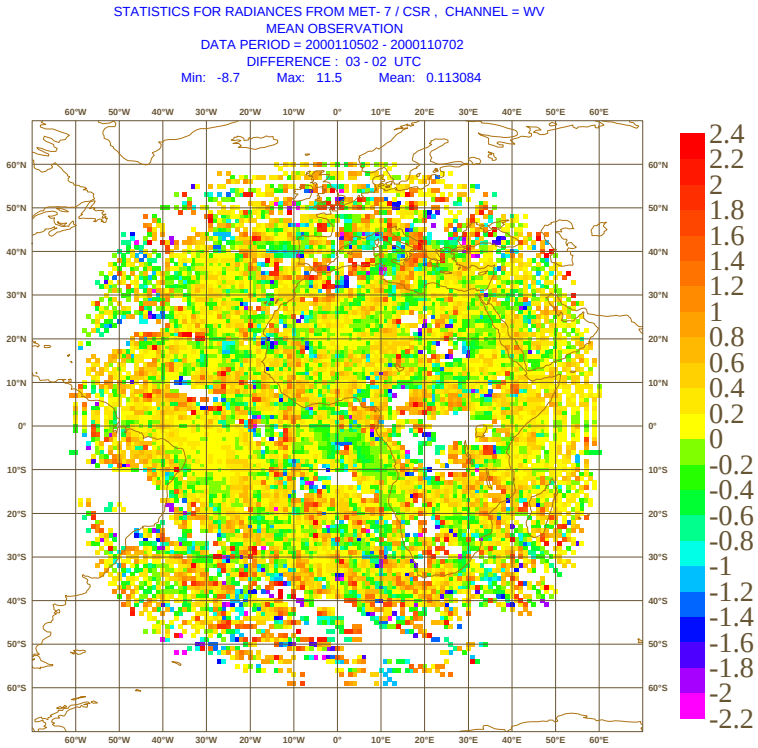


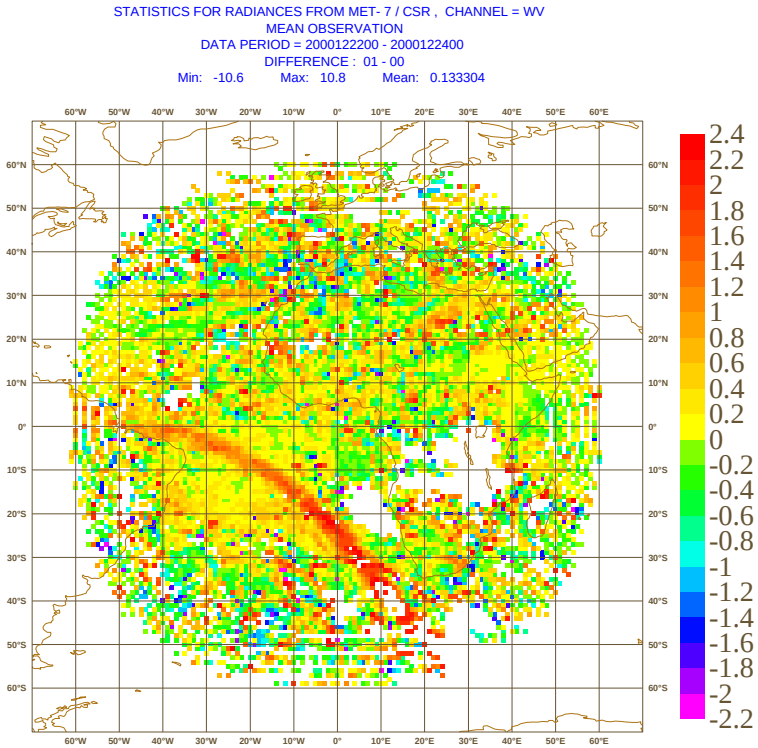


Figure 17: As Figure 7 but for: Top: 5–7 November 2000, 03 UTC minus 02 UTC. Bottom: 22–24 December 2000, 01 UTC minus 00 UTC.

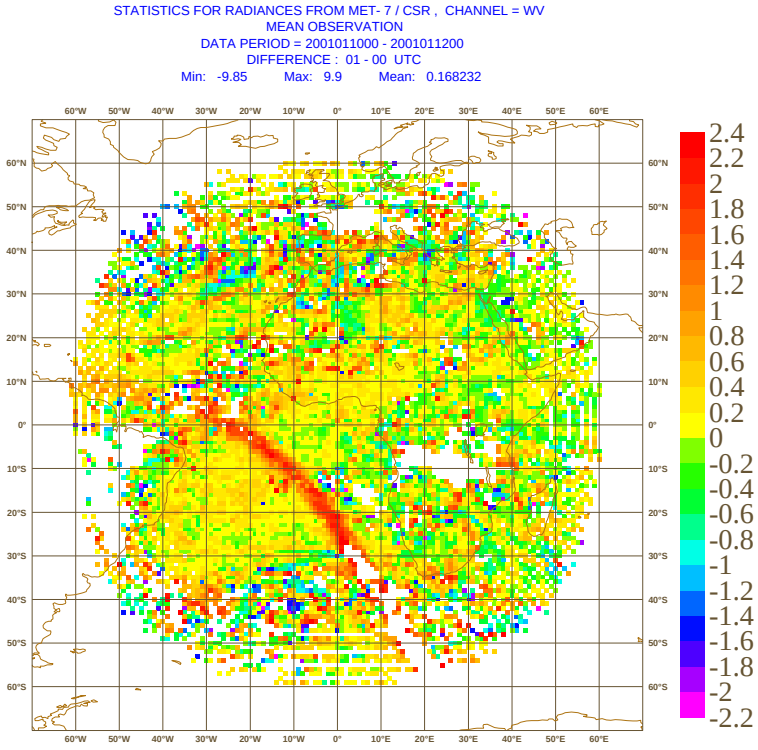


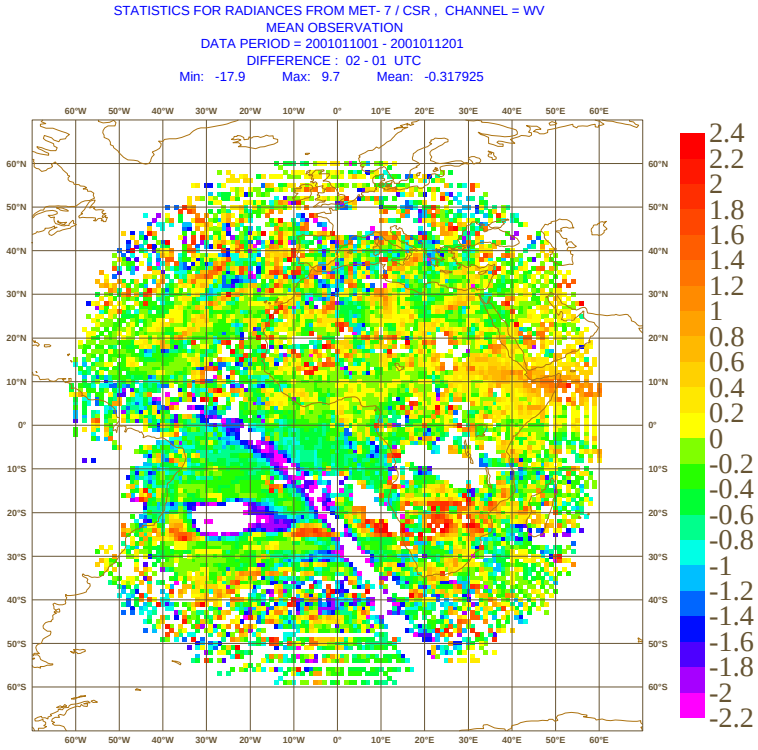


Figure 18: As Figure 7 but for 10–12 January 2001. Top: 01 UTC minus 00 UTC. Bottom: 02 UTC minus 01 UTC. (Note that differences in some anomalies exceed the colour scale, those areas appear white).

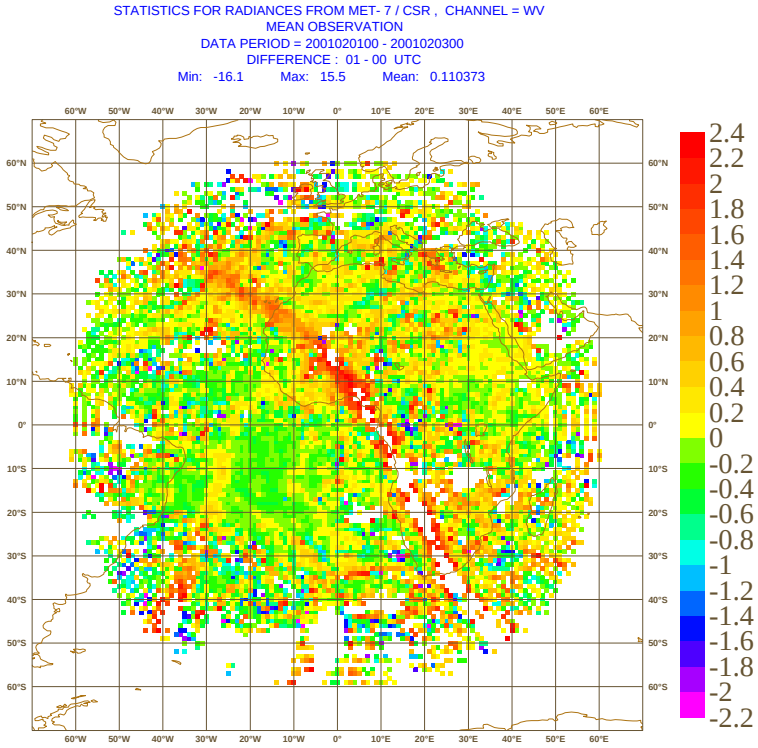


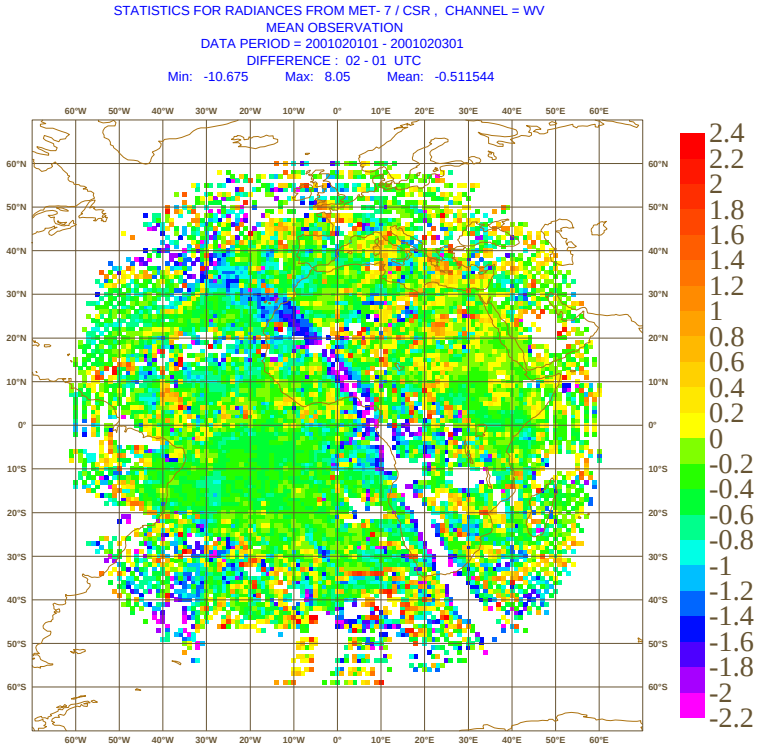


Figure 19: As Figure 7 but for 1–3 February 2001. Top: 01 UTC minus 00 UTC. Bottom: 02 UTC minus 01 UTC. (Note that differences in some anomalies exceed the colour scale, those areas appear white).

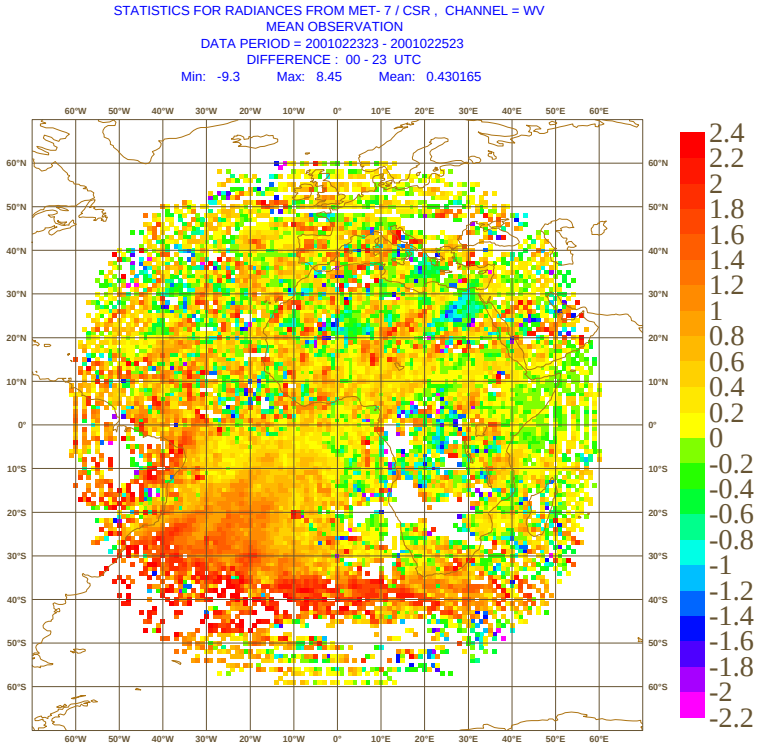


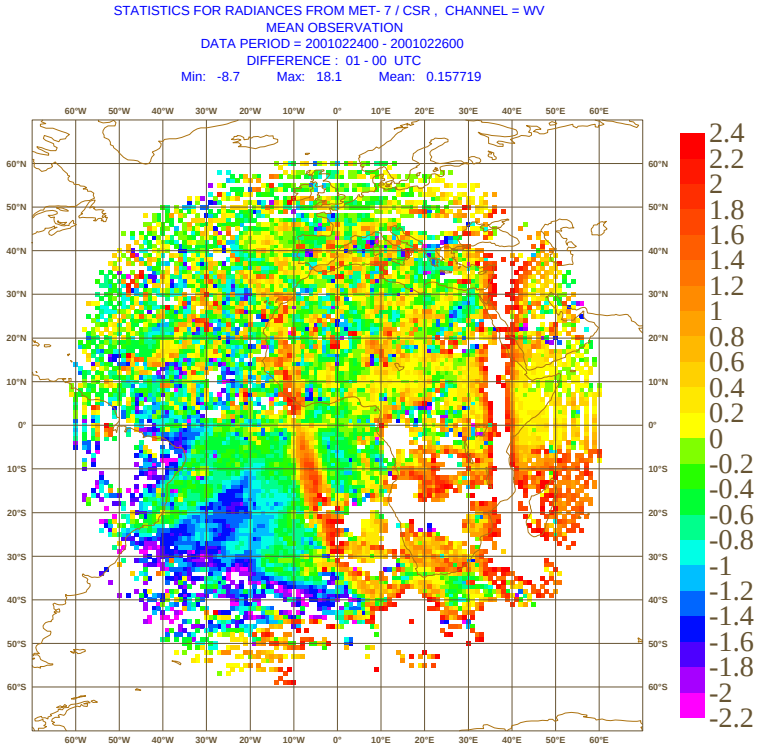


Figure 20: As Figure 7 but for 24–26 February 2001. Top: 00 UTC minus 23 UTC of previous day. Bottom: 01 UTC minus 00 UTC. (Note that differences in some anomalies exceed the colour scale, those areas appear white).

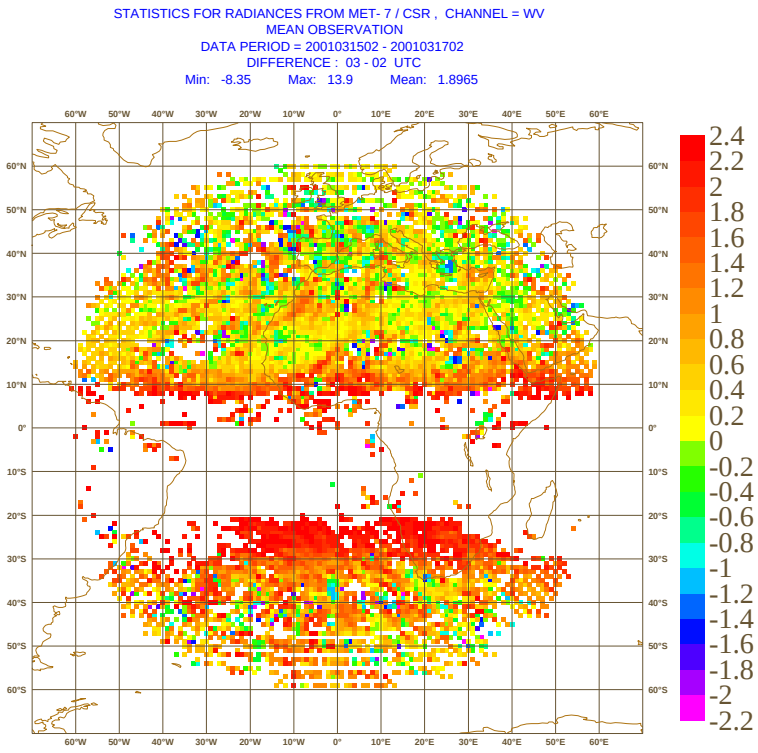


Figure 21: As Figure 7 but for 15–17 March 2001. 03 UTC minus 02 UTC.

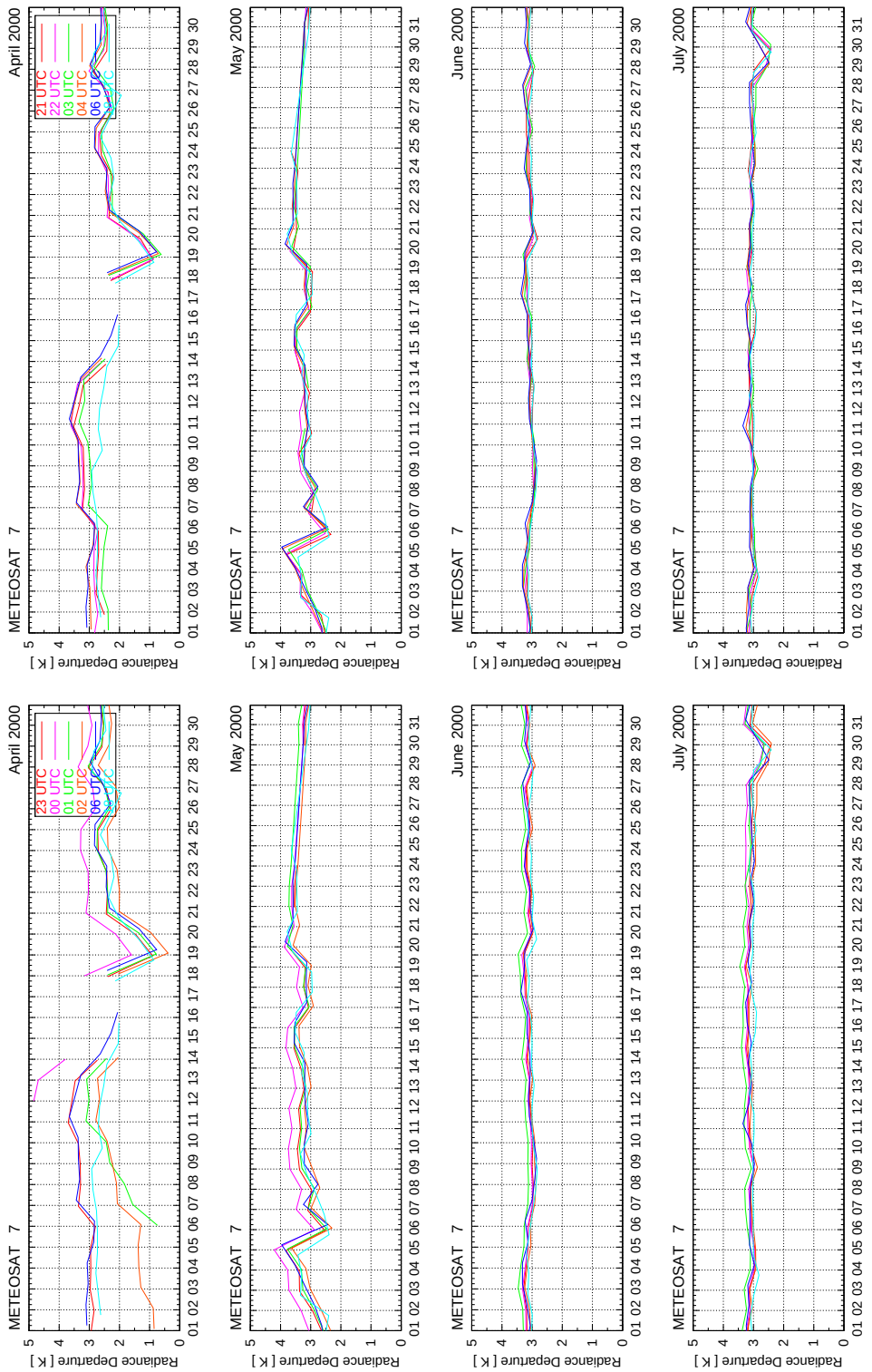


Figure 22: Time series of differences in WV clear–sky radiances from METEOSAT–7 and the corresponding forward calculations from ECMWF model FG for April 2000 to March 2001 for selected times of day (TB differences averaged over the whole satellite disk). Left: Hours close to midnight periodically strongly affected by solar stray light: 23 UTC (red curve), 00 UTC (magenta), 01 UTC (green), 02 UTC (yellow). Right: Hours farther from midnight: 21 UTC (red), 22 UTC (magenta), 03 UTC (green), 04 UTC (yellow). In all plots two hours not affected by stray light are added as a reference: 06 UTC (dark blue), 18 UTC (light blue).

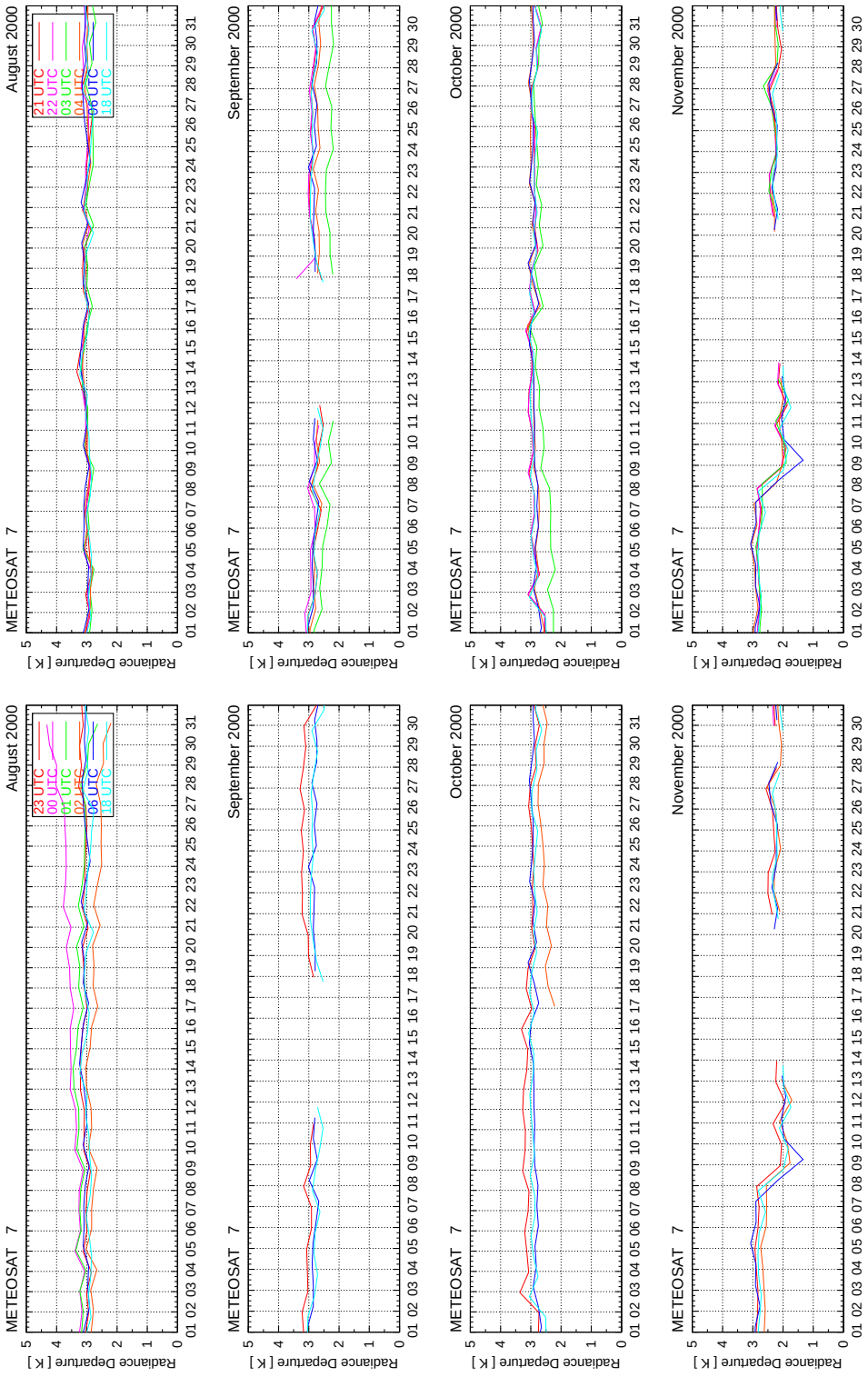


Figure 22: Continued.

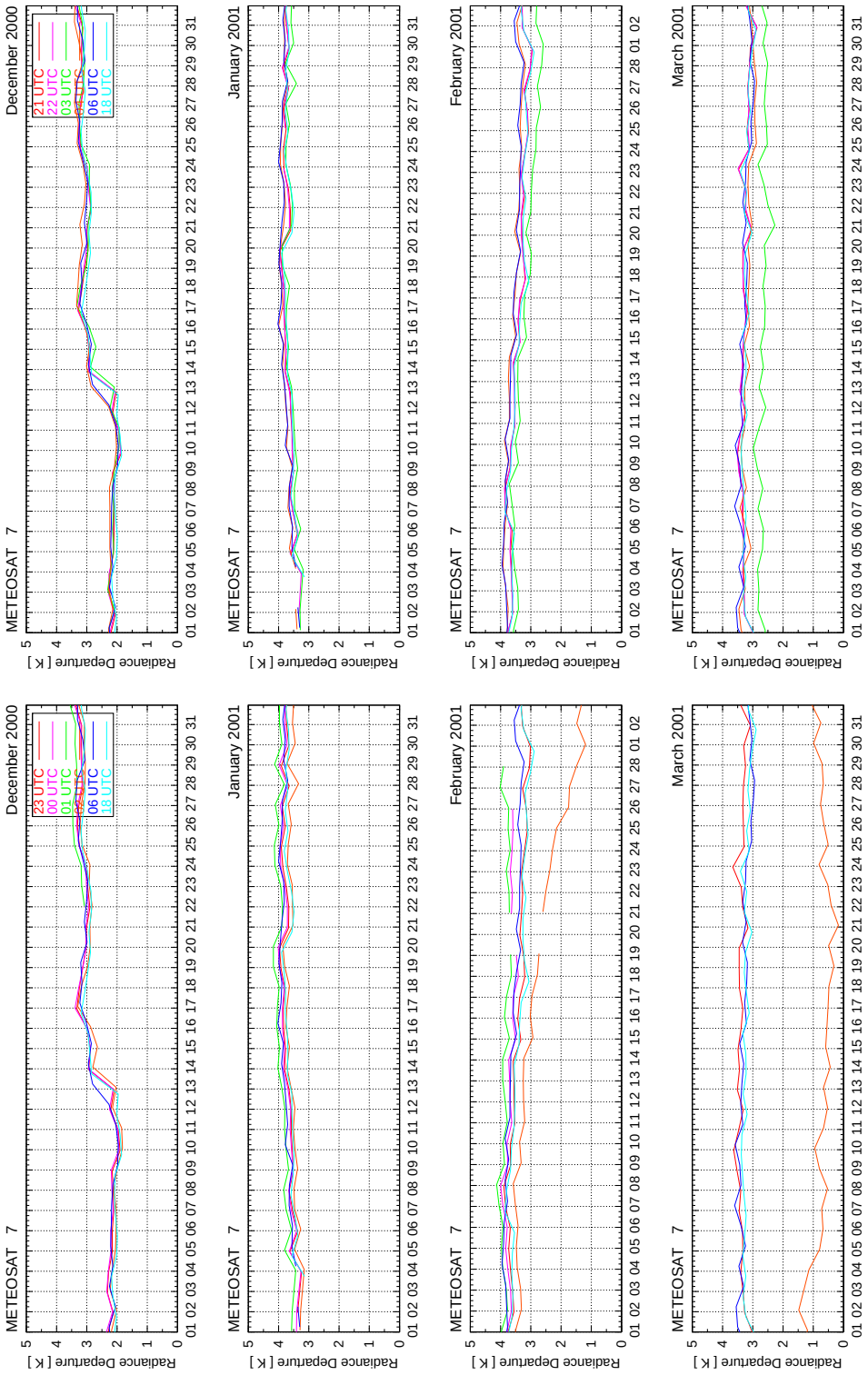


Figure 22: Continued.

Table 3: Periods during which some contamination of Meteosat–7 CSR is diagnosed from the ECMWF monitoring during the year April 2000 to March 2001 considered in this study. (Periods are chosen as to rather flag too many than too few images).

| | Anomalies Diagnosed in Monitoring | | |
|---|---|---|---|
| CSR slot | Spring Eclipse | | Autumn Eclipse |
| MET–7 | 2001 | 2000 | 2000 |
| 23 UTC | 08/03 – 31/03 | 01/04 – 13/04 | 27/08 – 20/10 |
| 00 UTC | 15/02 – 31/03 | 01/04 – 21/05 | 26/07 – 22/12 |
| 01 UTC | throughout the year | | throughout the year |
| 02 UTC | 20/01 – 31/03 | 01/04 – 21/05 | 26/07 – 08/11 |
| 03 UTC | 15/02 – 31/03 | 01/04 – 13/04 | 27/08 – 28/10 |

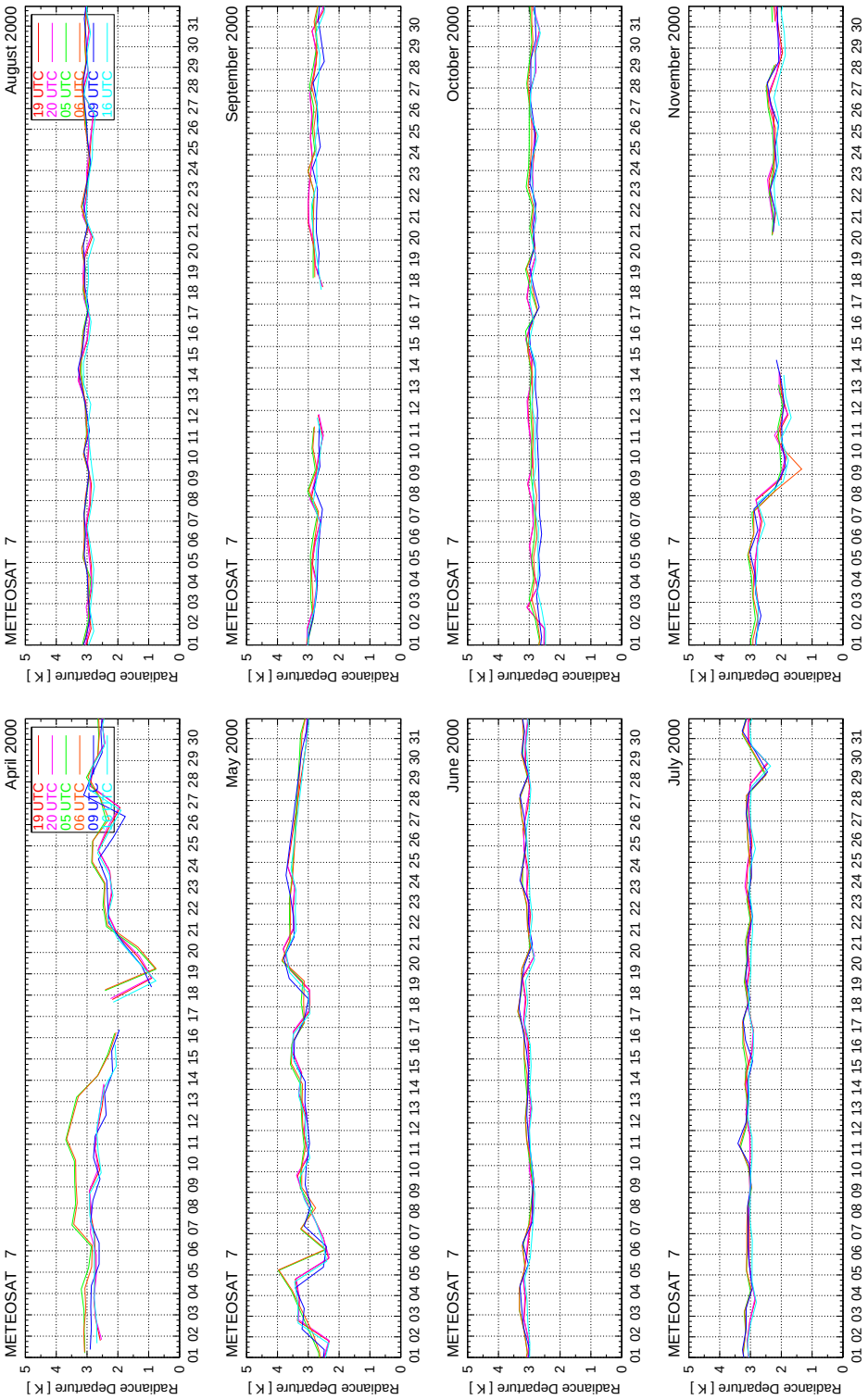


Figure 23: As Figure 22 but for hours during the day which are not affected by solar stray light: 05 UTC (green), 06 UTC (yellow), 09 UTC (dark blue), 16 UTC (light blue), 19 UTC (red), 20 UTC (magenta).

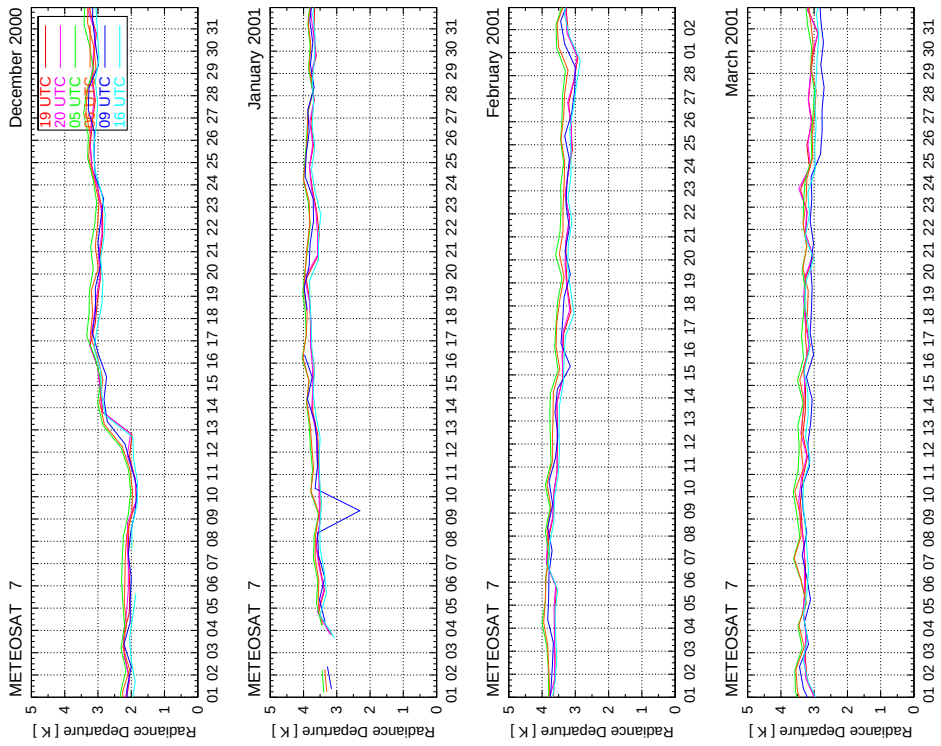


Figure 23: Continued.